Advances in MRI Around Metal

Pia M. Jungmann, MD,[1,2,3]* Christoph A. Agten, MD,[1,2]
Christian W. Pfirrmann, MD,[1,3] and Reto Sutter, MD[1,3]

The prevalence of orthopedic metal implants is continuously rising in the aging society. Particularly the number of joint replacements is increasing. Although satisfying long-term results are encountered, patients may suffer from complaints or complications during follow-up, and often undergo magnetic resonance imaging (MRI). Yet metal implants cause severe artifacts on MRI, resulting in signal-loss, signal-pileup, geometric distortion, and failure of fat suppression. In order to allow for adequate treatment decisions, metal artifact reduction sequences (MARS) are essential for proper radiological evaluation of postoperative findings in these patients. During recent years, developments of musculoskeletal imaging have addressed this particular technical challenge of postoperative MRI around metal. Besides implant material composition, configuration and location, selection of appropriate MRI hardware, sequences, and parameters influence artifact genesis and reduction. Application of dedicated metal artifact reduction techniques including high bandwidth optimization, view angle tilting (VAT), and the multispectral imaging techniques multiacquisition variable-resonance image combination (MAVRIC) and slice-encoding for metal artifact correction (SEMAC) may significantly reduce metal-induced artifacts, although at the expense of signal-to-noise ratio and/or acquisition time. Adding advanced image acquisition techniques such as parallel imaging, partial Fourier transformation, and advanced reconstruction techniques such as compressed sensing further improves MARS imaging in a clinically feasible scan time. This review focuses on current clinically applicable MARS techniques. Understanding of the main principles and techniques including their limitations allows a considerate application of these techniques in clinical practice. Essential orthopedic metal implants and postoperative MR findings around metal are presented and highlighted with clinical examples.
Level of Evidence: 4
Technical Efficacy: Stage 3

Within our aging society, there is an increasing prevalence of orthopedic metal implants. These include joint replacements of the hip[1] and knee[2] and of other joints such as the shoulder[3,4] or the ankle.[5] Other orthopedic devices of many different shapes and sizes include those for spine stabilization, arthrodesis, and fracture stabilization.[6] Although an uncomplicated postoperative course is common, patients may suffer from persistent or new complaints after surgery or may present with complications that involve the implant and the surrounding tissue.[7]

Suspected abnormalities such as aseptic loosening, pseudotumor formation, tumor, infection and abscess, fracture, nonunion or soft-tissue abnormalities[2,7–9] require further investigation in order to allow for appropriate treatment decisions. Besides patient history, physical examination, laboratory data, and plain radiography, magnetic resonance imaging (MRI) has become an important diagnostic modality during follow-up of metal implants.[10] While previously MRI close to metal implants was extremely challenging, a technological leap in recent years has made MRI of metal implants a major focus of musculoskeletal MRI.[8,11,12] Dedicated MR protocols have been developed that address a variety of clinical queries.

Metal artifact reduction sequences (MARS) aim to reduce artifacts from metal that superimpose the adjacent tissue.[13] MARS is a general term, which refers to no specific technique, but underlines the use of sequences optimized for imaging around metal. This review provides an overview of the physical background of metal artifact formation, the influencing factors, the optimization of conventional MR sequences, and the clinically applicable advanced MRI and reconstruction techniques. Advantages and disadvantages that occur with MARS will be discussed. Further, it focuses on clinical applications of MARS techniques, of which most are already available as product sequences. Typical and important implant-associated pathologies and complications

are demonstrated. In this review, safety issues will not be covered. The review is based on a PubMed-search using the terms "metal artifact MRI" and "metal artifact MR."

Metal Artifacts on MRI

Metal artifacts on MRI are mainly due to magnetic susceptibility differences between the metal implant and the surrounding tissue. Further mechanisms may impact the image quality, such as eddy currents induced within the metal by switched magnetic field gradients or locally induced radiofrequency fields.[14–16]

In order to perform MRI, a linear, homogenous main magnetic B_0 field is required for proper signal encoding and correct image reconstruction.[17,18] Since human soft tissue is mostly diamagnetic and metal implants are paramagnetic, or even ferromagnetic, sharp transitions in magnetic susceptibility exist between metal implants and the surrounding soft tissue.[9,13,19–22] These differences cause local susceptibility-related inhomogeneities of the main magnetic B_0 field, with rapid changes of the local magnetic field close to the implant. Therefore, the proton spins in these areas incorporate other frequencies than metal-free tissue would show. The proton spin frequency differences amount to 12–15 kHz at 1.5T and double at 3T.[23]

Due to the inhomogeneous B_0 field, three effects occur during MR image acquisition: 1) accelerated dephasing within a given voxel, 2) spatial misinterpretation of the signal, and 3) failure of frequency selective saturation pulses.[13] Accelerated dephasing causes signal loss in a voxel, typically resulting in a four-leaf clover artifact (dipole pattern). A distorted readout gradient field with erroneous frequencies results in wrong spatial encoding with pixel dislocation in the frequency-encoding direction. Erroneous frequencies manifest in signal loss (black), signal pile-up (white), geometric distortion ("in-plane" distortion: signal at an erroneous place within one plane; arrowhead appearance of artifacts) (Fig. 1), and failure of frequency selective fat suppression techniques.[11,24,25] For 2D multislice imaging, not only the frequency-encoding direction but also the slice-encoding direction uses the spin frequency for encoding. Therefore, the inhomogeneous B_0 field also results in a distorted slice-encoding gradient field with an erroneous slice profile ("through-plane" distortion involving adjacent slices; potato chip artifact) (Fig. 1).[25] The frequency-encoding gradient polarity has also been described to have an influence on the appearance of metal artifacts.[26] The phase-encoding direction is spared by the artifacts, since the relative phase of each phase-encoding step is not affected by a B_0 field offset.[27]

In contrast to computed tomography (CT) imaging, MRI artifacts are localized and are most severe adjacent to the implant.[9] Distant structures may be imaged with fewer or no restrictions. Prior to imaging, it needs to be estimated whether the area of interest will be obscured by artifacts.

In some circumstances, even standard MRI at 3T may be appropriate to address the clinical queries.[28] For example, in patients with unilateral hip replacements, contralateral hips may be assessed without dedicated MARS sequences.

Factors Influencing Artifact Formation

There are several factors that influence artifact formation. Artifact size depends on the implant itself, the MR field strength used (1.5T vs. 3T), the MR protocol, and the MR sequence parameters, including advanced metal artifact reduction sequences with dedicated image acquisition and reconstruction techniques (Table 1).[11] All parameters may be adjusted individually for every patient with his/her specific implant and clinical query. Patient compliance (long imaging times may not be possible due to motion artifacts or patient discomfort) as well as the infrastructure of each institution (1.5 vs. 3T scanner, new sequences, and advanced reconstruction techniques available) need to be taken into account when planning the MR examination.

Influence of the Implant

Implant material, size, configuration, and positioning influence artifact size on MRI.[18,29] A round symmetric cross-sectional area of the metal implant is of advantage, while complex shapes, in particular sharp edges, cause more severe artifacts. Spherical implants such as the head of hip prostheses cause the typical cloverleaf artifact (dipole pattern). The material of the implant most extensively influences the artifact size in both in-plane and through-plane directions (Fig. 2).[30] Nowadays, often titanium implants are used, which cause decidedly smaller artifacts on MRI as compared to cobalt-chromium, which again causes less severe artifacts than stainless-steel.[30–34] However, titanium may only be utilized in areas with minimal wear, while stainless-steel or cobalt-chromium are used when more wear-inducing movement is expected. Recent developments try to further reduce the magnetic susceptibility of titanium by synthesizing aluminum-free titanium composite material.[35] New materials are being tested to improve MRI around the metal implants further; for example, radiolucent carbon-fiber-reinforced polymers (CFRP), which were shown to have reduced artifacts on MRI as compared to titanium.[36–38] Other recently introduced materials are biodegradable magnesium alloys. These cause fewer artifacts than titanium and stainless-steel on CT and MRI.[38,39] However, even implants that cause more severe artifacts on MRI do not necessarily preclude proper radiological evaluation of the anatomic region, when imaging parameters are adjusted accordingly.[34,40]

Hardware and Pulse Sequences

Field Strength

Since the susceptibility-induced field inhomogeneity is doubled at 3T as compared to 1.5T, artifacts are less severe at
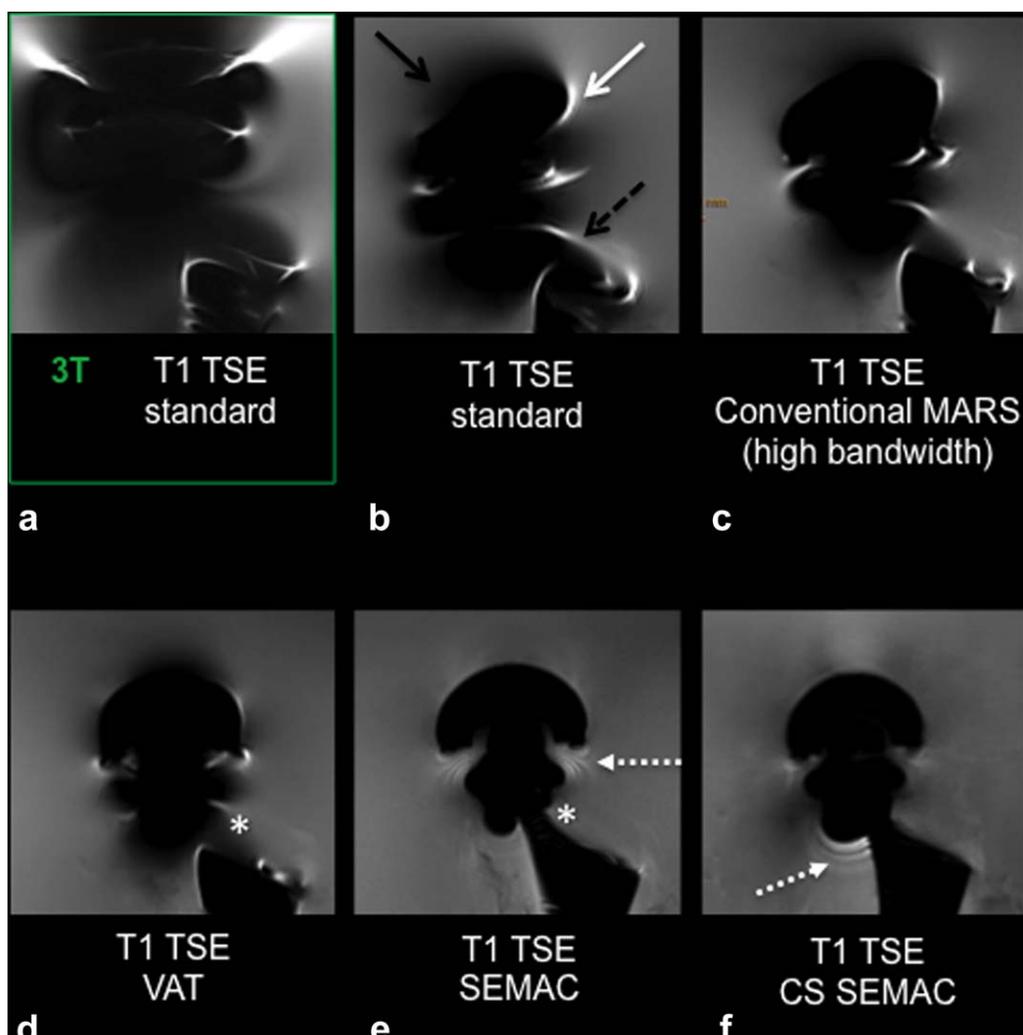
FIGURE 1: Metal artifacts on different MR sequences demonstrated in a total hip arthroplasty (THA) phantom at 3T (a) and 1.5T (b–f). Artifacts include signal-loss (solid black arrow), signal pile-up (white arrow) and geometric distortion (dashed black arrow). Artifacts are less severe if a 1.5T scanner (b) instead of a 3T scanner (a) is used. Conventional metal artifact reduction sequences (MARS) with high bandwidth allow a moderate reduction of metal artifacts (c). Advanced MARS techniques further reduce in-plane (view angle tilting; VAT; d) and through-plane (SEMAC; e) metal artifacts. The resolved through-plane artifacts using SEMAC techniques can be detected at the neck of the prosthesis, which is depicted on the correct plane only on SEMAC images (asterisk), but not on the other images. On SEMAC images small ring-artifacts can be depicted (dotted white arrow). Advanced reconstruction techniques including compressed sensing (CS; f) further reduce artifacts and reduce acquisition time. Typical more prominent ring-artifacts occur (dotted white arrow). In (e,f), there is no distortion seen and the shape represents the shape of the real implant. TSE, turbo spin echo.

1.5T (Figs. (1 and 3)). Therefore, when imaging a patient with metal implants, the straightforward way is using a 1.5T scanner. In general, metal artifact reduction techniques can be applied independent of field strength and reasonable artifact reduction is also possible at 3T.[13] However, with increasing artifact level at 3T, current artifact-reducing techniques are facing rigorous limits in various respects, such as the maximum power of the gradient and the radiofrequency (RF) transmit hardware or patient heating (high specific absorption rates, SAR). Obviously, imaging at even higher field strengths such as at 7T would further increase artifact size. Currently, for 7T imaging, implant materials are still being tested regarding MR safety. Certain implants may be acceptable, whereas others may not be safe at 7T.[41,42]

Among these potentially unsafe implants are endovascular grafts and several orthopedic implants.[41]

Positioning

Smaller artifacts are encountered when positioning the implant with the long axis parallel to the main magnetic field.[43–45] Exchanging phase-encoding direction and frequency-encoding direction may sometimes help to reduce artifacts, particularly if these cover one specific region of interest in the frequency-encoding direction.

Choice of Pulse Sequences

Gradient echo (GE) sequences show large regions of signal voids near metal due to intravoxel dephasing caused by B_0

TABLE 1. Overview of Clinically Applicable Conventional and Advanced Metal Artifact Reduction Sequences (MARS)

Conventional techniques
1.5T instead of 3T
Fast spin echo sequences instead of gradient echo sequences
Increasing receiver bandwidth
Increasing matrix size
Decreasing echo times
Switching frequency and phase encoding direction
Decreasing slice thickness
Fat saturation: STIR sequences; alternatives: Dixon sequences or subtraction images
Advanced techniques
View angle tilting (VAT)
Slice encoding for metal artifact correction (SEMAC)
Multi-acquisition variable-resonance image combination (MAVRIC)
Off-resonance suppression (ORS)
Advanced acquisition and reconstruction techniques.
Parallel imaging
Partial Fourier techniques/ undersampling
Compressed sensing

inhomogeneity. Spin echo (SE) sequences are much more robust due to the rephasing property of the refocusing pulse.[13,46] Turbo spin echo (TSE) sequences are well established due to their higher scan efficiency as compared to (single) spin-echo. T_1-weighted and intermediate (IM) weighted (w) TSE sequences with shorter echo times (TE) may show smaller artifacts than T_2-weighted sequences (with longer TE).[44,47] For IM-w sequences a TE of 35 msec may be used instead of 50 msec. With 3D sequences, the slice-encoding direction is also phase-encoded. Two variants have to be considered: nonselective and slab-selective excitation. For slab-selective excitation, the excited volume can be severely distorted in the through-plane direction.[18,44,48] 3D sequences with nonselective excitation show a very different behavior: due to the lack of an encoding gradient for slice-selection, no spatial misselection occurs. Still, all spins with frequencies outside the excitation bandwidth of the RF-pulse will not be excited and those regions will appear dark. For that reason, 3D nonselective sequences may be of advantage, in case pulses of sufficiently high bandwidth are applied.

Fat Suppression Techniques

Failure of fat saturation is another major problem encountered in the presence of metal implants.[49–51] The most commonly used spectral fat saturation is dependent on a homogenous magnetic field. Since spectral fat saturation relies on the fact that fat protons resonate at a fixed frequency being slightly offset from water protons, even small inhomogeneities of the B_0 field will prevent the saturation pulse to suppress the fat signal, or even worse, saturate the water signal instead (Fig. 4). Short tau inversion recovery (STIR) sequences are the sequences of choice for fat saturation when imaging around metal, since it is more resistant to B_0 inhomogeneities.[18,46] Using an inversion recovery technique, the fat signal is nulled based on its short T_1 relaxation time. The sequence design has to provide a matched bandwidth of inversion pulse and excitation pulse, otherwise field distortions may lead to different spatial positions of inverted and excited spins causing the STIR contrast to fail.[52] STIR results in a more homogenous fat saturation, at the expense of a lower signal-to-noise ratio
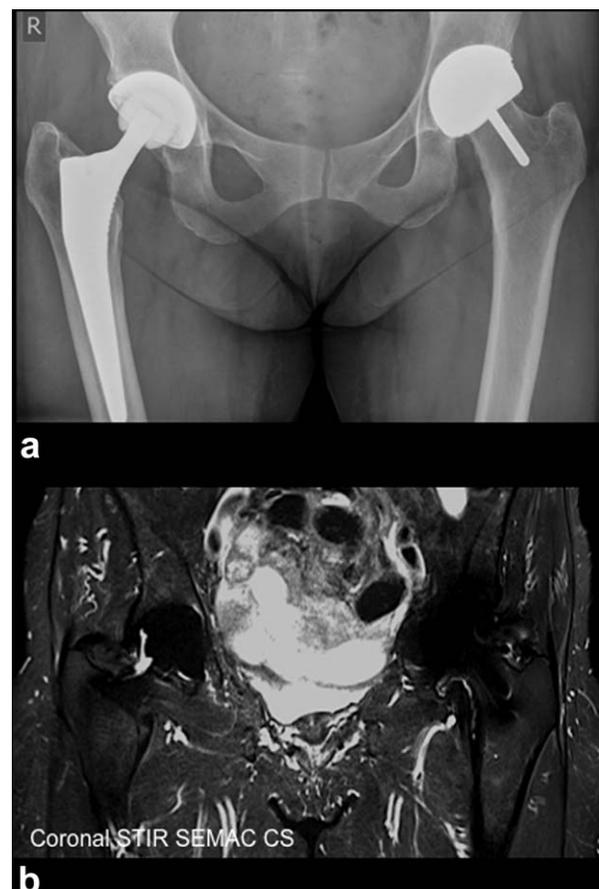

FIGURE 2: The severity of metal artifacts depends on the metal implant. While the standard total hip arthroplasty on the right (polyethylene-metal) only shows small residual artifacts, the resurfacing prosthesis (metal-on-metal) on the left shows severe surrounding signal-loss and distortion (same patient in a,b). STIR, short tau inversion recovery; SEMAC, slice-encoding for metal artifact correction; CS, compressed sensing.
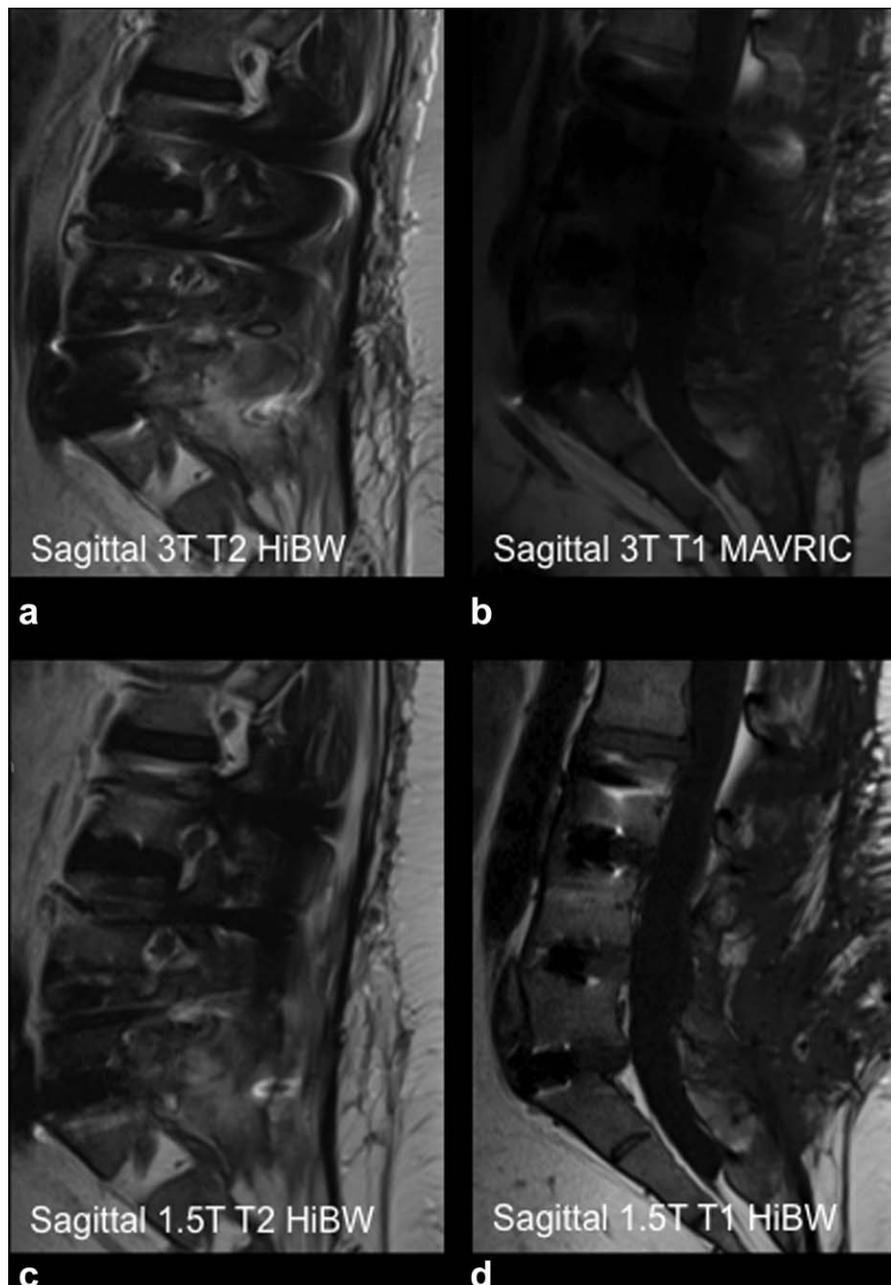
FIGURE 3: Patient with instrumentation and disc replacements of the lumbar spine. As compared to 3T images (upper row), 1.5T images (lower row) show fewer artifacts. The intervertebral foramina are less distorted with 1.5T (c) as compared to 3T (a). While at 3T even with advanced techniques (multi-acquisition variable-resonance image combination, MAVRIC) the spinal canal is obscured by artifacts (b), it may be evaluated at 1.5T on conventional MARS techniques with high bandwidth (HiBW) without difficulties (d).

(SNR). Some structures may be more difficult to evaluate on STIR sequences as compared to IM-weighted spectrally fat saturated sequences, such as cartilage or tendons.[44,52] Another disadvantage of STIR fat saturation is that it is not helpful for tissue evaluation after contrast administration, since contrast enhancing tissue may also be saturated due to its reduced T_1 relaxation time.

There are two other possibilities that may be applied after contrast administration. First, identical pre- and post-contrast T_1-weighted images may be subtracted. The subtraction images demonstrate the contrast-enhancing,

abnormal tissue nicely, with only minor obscuring artifacts, and it has been proven useful in clinical practice (Fig. 4).[53,54] This technique avoids additional artifacts caused by fat suppression techniques, but one needs to be aware of the fact that it does not eliminate geometric distortion artifacts occurring on the original images.

Second, Dixon TSE sequences (chemical-shift-based separation of water and fat signal) may be used, which only have a slightly longer acquisition time than standard TSE sequences.[55–60] Dixon techniques acquire separate in-phase and opposed-phase measurements and allow for secondary
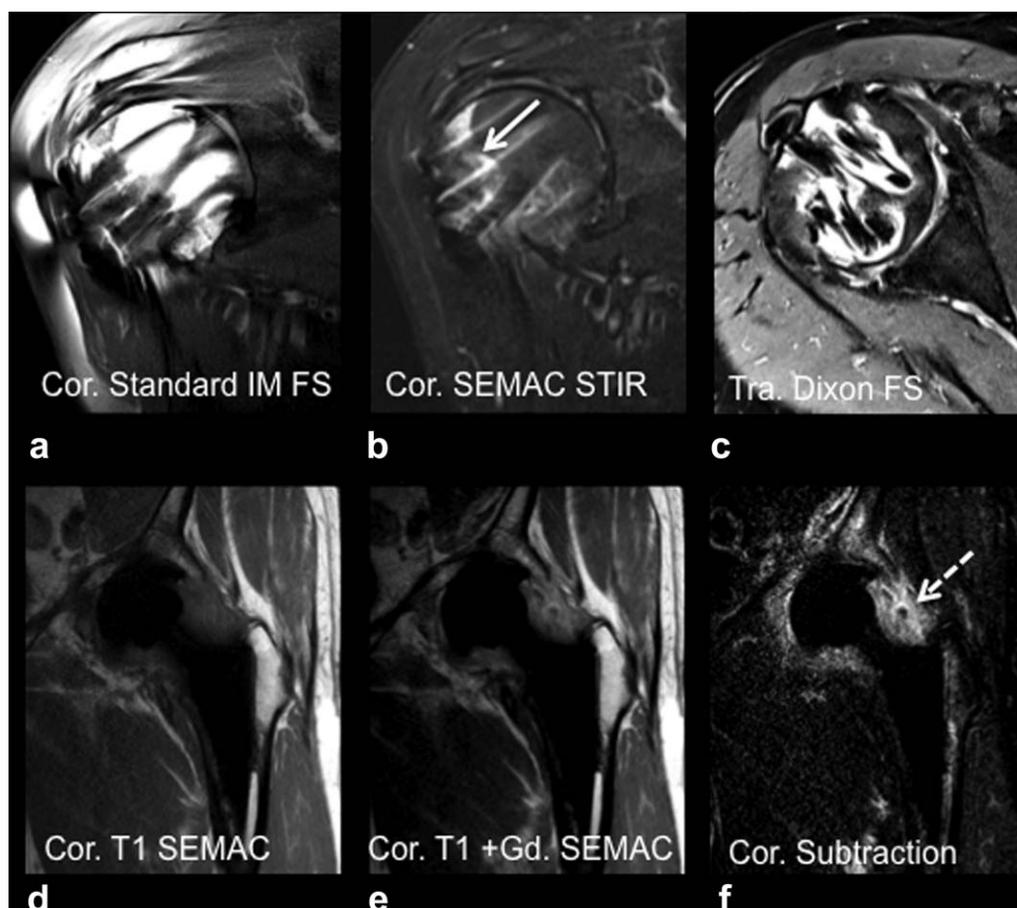
FIGURE 4: Fat saturation (FS) in the presence of metal artifacts. Upper row: patient with a PHILOS (Proximal Humeral Internal Locking System) plate for a humeral head fracture (solid white arrow). a: Since spectral fat saturation depends on a homogeneous magnetic field B_0 intermediate (IM)-weighted fat saturated images show major artifacts close to metal and the fracture line cannot be depicted. b: On STIR (short tau inversion recovery) images with SEMAC (slice-encoding for metal artifact correction), the fracture line is depicted properly. c: Dixon images with fat saturation show intermediate artifacts. d–f: Patient with a periprosthetic abscess at the neck of the total hip arthroplasty (dashed arrow). Subtraction of the noncontrast T_1-weighted image from the T_1-weighted image after administration of gadolinium (Gd.) shows strong contrast enhancement and may replace fat saturation in some cases. Cor., coronal; Tra., transverse.

water-only and fat-only image reconstructions.[50,60] Images may be reconstructed with and without fat suppression. In contrast to spectral fat saturation, Dixon is less sensitive to magnetic field (B_0 and B_1) inhomogeneities; moderately varying field inhomogeneities can be corrected in the reconstruction.[60] The robustness of the Dixon fat suppression against metal artifacts is intermediate (fewer artifacts than with spectral fat saturation, worse artifacts than with STIR techniques). Dixon techniques may be used as fat-saturated T_1-weighted sequence after contrast administration.[55,56] IM-w Dixon sequences may be used instead of STIR.[56] Although STIR works better for fat suppression in the presence of metal implants, the advantage of Dixon sequences is a high SNR and the production of both in-phase and fat-suppressed sequences within a single acquisition.[55]

Conventional MR Pulse Sequence Optimization

As a first step, the existing conventional MR sequences should be optimized when scanning patients with metal implants by adapting basic acquisition parameters. Frequently, this optimization is already sufficient for routine clinical use, for example, for standard titanium implants at 1.5T. Measures to reduce artifacts address in-plane as well as through-plane artifacts. These include possibly switching frequency and phase-encoding direction, increasing the bandwidth of the receiver or transmit pulses, increasing the matrix size for in-plane artifact reduction, and reducing the slice thickness for through-plane artifact reduction.[25,49] Using high-bandwidth RF pulses has also been shown to substantially reduce through-plane distortion artifacts, at the cost of an increased blurring.[61] In contrast to previous assumptions, new studies have shown that longer echo trains do not reduce metal artifacts.[62]

When applying these adjustments, one needs to keep in mind that increasing the readout bandwidth or increasing the resolution (either in-plane or thinner slices) will reduce the SNR, which needs to be compensated by longer scan times. Further, large RF bandwidths and short echo spacing

lead to high SAR, in particular for TSE sequences exposing long echo trains of refocusing pulses, which may cause heating of the patient.[12] Additionally, larger ranges of signal frequencies potentially cause more frequency-encoding problems. If the SAR exceeds critical thresholds it may need to be addressed by reducing the flip angle (60–130° rather than 180° refocusing pulses; again resulting in lower SNR), using longer repetition times (resulting in longer scan times and potentially altered MR contrast), or by reducing the number of slices.[63] Therefore, there is a trade-off between the different aims during clinical image acquisition. The decision on which exact sequence to use in the specific case often needs to be made individually, depending on the localization, size, configuration, and material of the implant, on the query, the patients cooperation, and on scanner availability.

RECEIVER BANDWIDTH. A very efficient measure for reducing in-plane artifacts in conventional MR sequences is increasing the receiver bandwidth.[52,62,64] If stronger imaging gradients are applied, each voxel is encoded by a wider frequency range.[44] Thus, local frequency errors have less impact on the spatial encoding, ie, the translation of a certain frequency to the spatial position of the spin. Therefore, a higher bandwidth reduces signal misregistration in the in-plane frequency-encoding direction. This means the shift of spins with wrong frequencies in the image is reduced. Yet high bandwidths need strong gradients, which are sometimes the limiting factor. Doubling or tripling the bandwidth to 500–800 Hz/pixel is recommended, although this substantially reduces the SNR.[64] Consequently, the scan averages may need to be increased to receive enough signal, which increases the scan time. On the other hand, using a high bandwidth allows the echo spacing to be reduced, resulting in less T_2 decay with less signal loss. However, these lead to higher SAR, which limits this approach.[65] The bottom line is that increasing readout bandwidths reduces artifacts significantly, with a relevant SNR loss and without increased scan time when applied thoughtfully. For many clinical situations, using increased readout bandwidth is considered to be the most effective parameter for artifact reduction.[62]

MATRIX SIZES. Further, for in-plane artifact reduction, increasing the image resolution (increased matrix size at constant field of view) reduces both in-plane distortions and intravoxel dephasing.[66] Matrix sizes of 512 are recommended. The matrix increase is most efficient when performed in the frequency-encoding direction. To limit truncation artifacts the phase-encoding direction should at least have 60–80% of the matrix size of the frequency-encoding direction.[9]

SLICE THICKNESS. Reducing the slice thickness, implicating a stronger slice selection gradient, aims to reduce through-plane distortion. As a result, wrong frequencies affect a smaller anatomic diameter in slice-encoding direction. Sometimes a slice thickness of 4 mm is sufficient (eg, for transverse spine imaging or tumor prostheses), but 3.5 mm or 3 mm improves artifact reduction further. Obviously, reducing the slice thickness increases scan time and reduces SNR again.
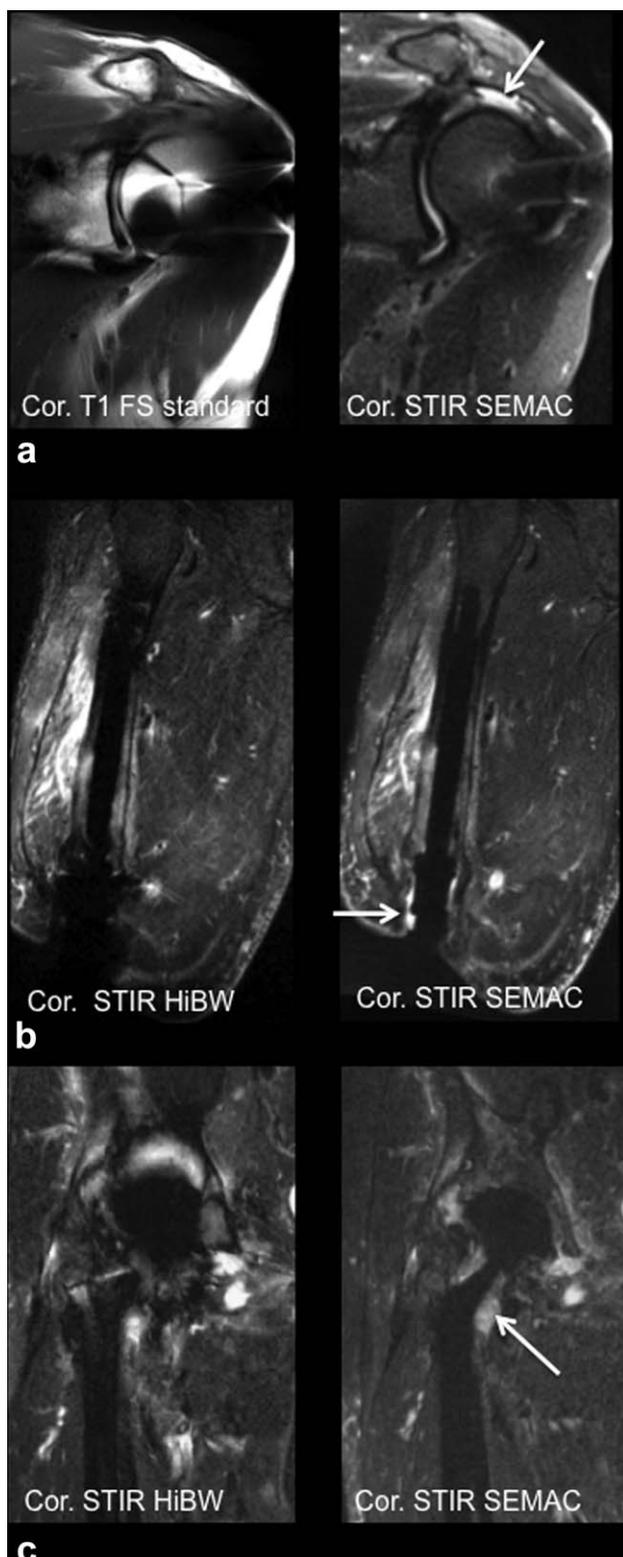
Specialized MARS Techniques

Since MRI around metal became an important clinical tool, efforts were made in recent years to develop dedicated MRI techniques. These have allowed drastically reducing residual metal artifacts. Techniques that are clinically applied and available to date are view-angle-tilting (VAT)[67] and multispectral imaging (MSI) that include multiacquisition variable-resonance image combination (MAVRIC)[68] and slice-encoding for metal artifact correction (SEMAC; combined with VAT).[7,17,25,32,69–72] A combination of the latter two techniques have been reported as MAVRIC-SL[70] and MSVAT-SPACE.[71] General Electric (GE, Milwaukee, WI) calls its sequences with these dedicated MARS techniques "MAVRIC" (conventional MARS techniques plus MAVRIC) and "MAVRIC-SL (selective)" (MAVRIC/SEMAC hybrid). Philips (Best, Netherlands) calls its dedicated MARS techniques "O-MAR" (conventional MARS techniques plus VAT) and "O-MAR XD" (O-MAR plus SEMAC). Siemens (Erlangen, Germany) calls its dedicated MARS techniques "WARP" (conventional MARS techniques plus VAT) and "advanced WARP" (WARP plus SEMAC) (in alphabetic order).[25,69,70,72]

The efficacy of these advanced metal artifact reduction techniques with respect to artifact reduction as compared to conventional sequences has been demonstrated in several studies (Fig. 5).[7,71,73] They are available for 1.5T and 3T.[74] However, unless the field inhomogeneities are very mild, artifact size is smaller and artifact reduction is more effective at 1.5T; therefore, overall image quality in patients with metal implants is superior at 1.5T (Fig. 3).[73,75,76] By applying these advanced techniques in clinical practice, a sufficient in-plane and through-plane metal artifact reduction is achieved for most types of modern metal implants. Interleaved spectral bin acquisition strategies are being developed for overlapping MSI techniques that allow for flexible choice of the repetition time without any relevant crosstalk impact.[77] It was described that both SEMAC and MAVRIC significantly reduce artifact extent compared to conventional sequences and that SEMAC and MAVRIC achieved similar artifact reduction.[78] Serious drawbacks in using these standard versions of these techniques are long acquisition times, a significantly reduced SNR, and reduced spatial resolution and contrast.[79] These can be addressed by using advanced

acquisition techniques with undersampling and advanced reconstruction techniques, as described below in more detail.

VIEW ANGLE TILTING (VAT). For VAT an additional compensatory, slice-selection gradient is applied simultaneously with the conventional readout gradient.[7,71,80] This

Cor. T1 FS standard   Cor. STIR SEMAC

a

Cor. STIR HiBW   Cor. STIR SEMAC

b

Cor. STIR HiBW   Cor. STIR SEMAC

c

gradient causes a tilting of the read-encoding dimension towards the slice selection dimension (ie, the angle from which the excited slice is viewed is tilted) and thus a "shearing" of the voxels. Consequently, all off-resonance induced shifts along the readout direction within the excited slice are eliminated. The view angle depends on the ratio of slice gradient and readout gradient, which in turn depend on slice thickness, bandwidth of the RF pulse, and readout bandwidth. VAT does not increase scan time, but the slice shear induces some blurring.[80] Using thin slices may keep the blurring at an acceptable level. The main limitation of VAT is that it does not correct for through-plane distortions. However, VAT plays an essential role in the implementation of the SEMAC technique.

SLICE-ENCODING FOR METAL ARTIFACT CORRECTION (SEMAC). SEMAC is used in combination with VAT. In addition to in-plane artifacts, SEMAC reduces through-plane distortions by correcting for signal that is excited in wrong slice positions.[71,72,81] SEMAC is based on a 2D TSE sequence. Through-plane distortion correction becomes possible by applying additional phase-encoding steps (gradients) in the third dimension (slice selection) to register distortions for each individual slice. As in 2D sequences, single slices are excited with an RF pulse with the shape of minimally overlapping boxcar profiles, but the additional phase-encoding resolves a larger 3D slab around each slice position, which could be called a pseudo-3D acquisition. The information on slice distortion is used to correct the distortion of the acquired slice and adjacent slices during postprocessing.[72] In SEMAC, the entire slice profile is coded and analyzed for each slice individually. The required coverage of this pseudo-3D acquisition is dependent on the extent of the geometric distortion caused by the metal implant. Exemplarily, while for some implants seven SEMAC steps may be sufficient since the through-plane distortion only involves the adjacent three slices, for stainless-steel or complex implants, 13 or even more SEMAC steps may not be sufficient to account for the entire through-plane distortion.[7,32] The amount of SEMAC steps may be chosen

FIGURE 5: Clinical impact of advanced metal artifact reduction techniques. SEMAC (slice-encoding for metal artifact correction) images demonstrate abnormal findings (arrows) next to metal implants that are not visible on standard sequences (a) or conventional metal artifact reduction sequences with high bandwidth (HiBW) (b,c). a: Supraspinatus tendon re-tear in a patient with small screws in the greater tubercle after rotator cuff repair. b: Periprosthetic fluid collection in a patient with infection around an endo-exo-prosthesis of the thigh after amputation. c: Abscess formation at the neck of a total hip arthroplasty, which cannot be differentiated from artifacts on high bandwidth STIR images but can be correctly identified on STIR-SEMAC images. FS, fat saturated; HiBW, high bandwidth; STIR, short tau inversion recovery; SEMAC, slice-encoding for metal artifact correction; Cor., coronal.

individually for each scan. The larger the area of field inhomogeneities, the more slice-encoding steps need to be selected.[82] Reducing these steps reduces scan time. Still, the 3D encoding of each slice is obviously very time-consuming, even though the increased SNR can be employed to use undersampling techniques such as partial Fourier and parallel imaging. A residual ripple artifact was described as typical for SEMAC sequences, which may effectively be addressed with slice overlap at an additional scan-time penalty (Fig. 1).[83] It was demonstrated in several studies that SEMAC is superior to standard MR sequences, high bandwidth protocols, and simple VAT with respect to artifact reduction.[1,2,84,85]

MULTIACQUISITION VARIABLE-RESONANCE IMAGE COMBINATION (MAVRIC). MAVRIC is a spatially nonselective 3D acquisition technique to reduce metal artifacts.[4,30,70] The 3D phase-encoding does not suffer from through-plane distortions, as is the case for any gradient based slice-selection. However, a single nonselective excitation pulse may not cover the full range of off-resonant frequencies near metal implants, meaning those spins are not excited and will appear dark in the image. MAVRIC solves this problem by acquiring several 3D slaps multiple times with discretely varying resonance frequency offsets (so-called spectral bins). The shape of the MAVRIC RF pulse resembles Gaussian profiles.[25] All entire 3D slaps are finally combined and analyzed during postprocessing in order to build an artifact-reduced composite image.[25] A potential disadvantage of MAVRIC is aliasing in the through-plane direction due to the spatially nonselective 3D volume excitation, particularly when imaging the hip or shoulder joint.[44]

MAVRIC-SL applies a selective excitation pulse and shares the same approach for through-plane artifact reduction as SEMAC. MAVRIC-SL excites singles slices like SEMAC but uses the pulse profiles from MAVRIC.[69,70] Not only standard TSE sequences and STIR, but also ultrashort echo time sequences (UTE)[86] are compatible with MAVRIC. Using an undersampled 3D radial UTE-MAVRIC sequence, imaging of tissues with short T_2 such as tendons, ligaments, and cortical bone has been described as feasible adjacent to metallic implants.[87]

OFF-RESONANCE SUPPRESSION (ORS). Efforts have been made to improve MSI sequences further, such as by combining SEMAC (ORS-SEMAC) and MAVRIC (ORS-MAVRIC) with off-resonance suppression.[88] In ORS the RF bandwidths and gradients of the excitation and the refocusing pulses are different. Only those spins that are in the range of both pulses contribute to the image. ORS limits the selected spatial-spectral selectivity in multispectral MRI. With ORS-SEMAC fewer phase-encoding steps are required compared with the standard SEMAC. Thus, ORS contributes to alias-free imaging with scan-time reduction and flexibility of scan-orientation.[88] Disadvantages of ORS include signal voids and loss of homogeneity.[88]

OTHER TECHNIQUES. Several other dedicated MARS techniques have been developed, which however, have not yet been shown to be clinically feasible and feature a low spatial resolution or long acquisition times. These include prepolarized MRI (PMRI),[89] single-point imaging (SPI),[90] field mapping,[54] sweep imaging with Fourier transformation (SWIFT),[91] bSSFP banding artifact correction,[92–96] dual-reversed-gradient acquisitions,[97] and short echo-time projection reconstruction acquisitions.[25]

ADVANCED ACCELERATION TECHNIQUES. Besides optimizing dedicated metal artifact-reducing techniques, an additional or complementary approach is to optimize postprocessing image reconstruction techniques. Such as for CT imaging, also for MRI, advanced reconstruction algorithms including iterative reconstruction implemented in postprocessing are being developed.[98] These aim to decrease artifacts further, increase image resolution, increase SNR, optimize image quality, and reduce scan time with optimized postprocessing algorithms in combination with advanced image acquisition techniques such as partial Fourier, undersampling, parallel imaging, SEMAC, and MAVRIC. This is of particular importance in order to reduce the extremely long acquisition times of SEMAC and MAVRIC to clinically feasible scan times.[99]

Advanced acquisition and reconstruction algorithms used in combination with SEMAC are sparsity-driven and compressed-sensing (CS)-based *k*-space undersampling of SEMAC data with iterative reconstruction (CS-SEMAC).[98–101] CS-SEMAC uses the redundant, distorted information gained with the MSI acquisition for image optimization and allows reduction of the scan time by the use of undersampling.[98] Using CS, the phase-encoding steps may be reduced, resulting in an 8-fold acceleration of *k*-space-encoding and in a dramatic reduction of the acquisition time.[99,102] Image quality with CS-SEMAC is comparable to SEMAC sequences, but with a scan time of 4–5 minutes instead of 10–12 minutes, which drastically increases the clinical applicability.[99] Still, these algorithms are very demanding in terms of numerical computation power and need long reconstruction times. Further, by exploration of missing image information, by smoothening the image and enhancing the contrast, a somewhat artificial impression of the image may occur.

Clinical Application

Clinical Relevance

Clinical relevance of MARS sequences and an impact on treatment management have been demonstrated in several studies (Fig. 5).[7,84,103] Inclusion of MAVRIC or SEMAC to the imaging protocol allowed determining the need for surgery, and the type of surgery.[103,104] Exemplary MR protocols for the spine, hip, and knee are presented in Table 2.

TABLE 2. Exemplary MR Protocols for Patients With Metal Implants at the Spine, Hip, and Knee

Spine pulse sequences	Coronal STIR	Sagittal T2	Sagittal T1	Transverse T2	Sagittal T1 Dixon
Advanced MARS techniques	VAT	—	—	—	—
Repetition time (msec)	4350	3000	500	3000	612
Echo time (msec)	44	100	7.7	90	11
Slice thickness (mm)	4	4	4	4	4
Distance factor (%)	20	10	10	20	10
Refocusing flip angle (°)	150	150	150	150	150
Field of view (FOV; mm)	320	300	300	225	300
Pixel size (mm)	1.0×1.0	0.7×0.7	0.7×0.7	0.5×0.5	0.8×0.8
Bandwidth (Hz/ Pixel)	504	507	507	587	303
Averages	1	3	3	2	2
Turbo factor	15	18	3	15	3
Inversion time (msec)	170	—	—	—	—
Number of slices	15	15	15	5	15
Slice-encoding steps	—	—	—	—	—
Phase encoding direction	F≫H	H≫F	H≫F	A≫P	H≫F
Acquisition time (min:sec)	2:03	4:53	4:29	2:41	3:57
Hip pulse sequences	**Coronal STIR**	**Coronal T2**	**Sagittal T1**	**Transverse STIR**	**Transverse T1 Dixon**
Advanced MARS techniques	SEMAC CS	—	—	—	—
Repetition time (msec)	4570	4000	550	4000	463
Echo time (msec)	36	58	7.3	31	11
Slice thickness (mm)	4	4	4	7	5
Distance factor (%)	0	50	10	25	25
Refocusing flip angle (°)	140	150	180	150	135
Field of view (FOV; mm)	300	220	200	180	180
Pixel size (mm)	1.2×1.2	0.4×0.4	0.6×0.6	0.5×0.5	0.6×0.6
Bandwidth (Hz/ Pixel)	501	391	434	449	391
Averages	1	2	2	3	1
Turbo factor	9	15	3	11	3
Inversion time (msec)	160	—	—	150	—
Number of slices	29	20	29	27	33
Slice-encoding steps	13	—	—	—	—
Phase encoding direction	R≫L	R≫L	A≫P	A≫P	A≫P
Acquisition time (min:sec)	5:12	2:36	3:34	3:54	3:56
Knee pulse sequences	**Coronal STIR**	**Coronal T1**	**Sagittal IM**	**Transverse STIR**	
Advanced MARS techniques	SEMAC	—	SEMAC CS	—	
Repetition time (msec)	4500	491	4380	5420	
Echo time (msec)	39	11	36	31	

TABLE 2: Continued

Knee pulse sequences	Coronal STIR	Coronal T1	Sagittal IM	Transverse STIR
Slice thickness (mm)	4	3	3	3.5
Distance factor (%)	0	20	0	10
Refocusing flip angle (°)	150°	180	150	180
Field of view (FOV; mm)	200	170	170	170
Pixel size (mm)	0.6×0.6	0.4×0.4	0.5×0.5	0.4×0.4
Bandwidth (Hz/ Pixel)	539	429	601	395
Averages	1	3	1	2
Turbo factor	17	3	11	17
Inversion time (msec)	160	—	—	160
Number of slices	27	24	34	39
Slice-encoding steps	8	—	15	—
Phase encoding direction	R≫L	R≫L	A≫P	R≫L
Acquisition time (min:sec)	4:54	3:23	4:33	5:00

MARS, metal artifact reduction sequences; STIR, short tau inversion recovery; CS, compressed sensing; IM, intermediate weighted.

Several abnormalities around orthopedic implants may be visualized by using MARS sequences.[49,105] Aseptic loosening of an implant is characterized by a circumferential lucency around the implant or the cement, which is progressively enlarging over time,[44,105] while an osteolysis has a more localized extent (Fig. 6).[106] There is an ongoing debate whether radiography, MRI, or CT is more accurate with respect to detection of loosening and osteolysis.[106–109] With improving techniques MRI may become more sensitive.[109] With metal-on-metal total hip arthroplasty (THA) and the associated major risk of adverse local tissue reactions (ALTR), MARS gained importance.[53,110–115] But also with other types of orthopedic implants the so-called "pseudotumors," initiated by excessive wear, may be observed.[7,113,115,116] Periprosthetic infection, fluid collections, and abscesses or osteomyelitis are further severe complications that require prompt treatment. Nonimplant associated soft-tissue abnormalities may be found on MARS sequences, such as cartilage defects, tendon tears, muscle atrophy and fatty infiltration, meniscal or labral lesions, disc abnormalities, spinal canal stenosis, neural injury, or pathology.[49,105,117,118] Recurrence of a tumor or a newly developed tumorous formation is another important clinical entity where MARS sequences may be utilized, both for detection and classification of findings.[7,119,120]

Spine
For metal artifact reduced imaging of the spine, the frequency-encoding direction should be positioned along the long axis of the pedicle screws in sagittal and transverse images (anterior–posterior).[121] The utility of SEMAC for artifact reduction in spine imaging has been demonstrated in several studies.[84,121–126] SEMAC sequences enabled significantly improved periprosthetic visualization of the pedicles, vertebral body, dural sac, and neural foramina.[84] Still, acquisition of MARS spine images with diagnostically sufficient SNR and contrast is challenging.[51] STIR sequences sometimes fail to detect bone marrow edema, and therefore evidence of bone marrow edema should be assessed with caution in the presence of metal.[127,128] Compressed sensing MSI techniques are promising and show improvements with respect to nerve visualization, artifact reduction, and image quality.[98] It was reported that even T_2-weighted 3D imaging in functional end positions of the cervical spine were possible in the presence of metal implants, with good visualization of spinal canal narrowing.[48]

Tailored choices of sequences are very useful for spine imaging, depending on the type of implant or instrumentations. The image quality of spine MRI heavily depends on the type of metal used. While standard titanium dorsal stabilization only cause minor artifacts, some disc replacements cause severe artifacts. Imaging of two or three stabilized bodies is frequently feasible with high bandwidth sequences, even without the use of dedicated MSI techniques. In contrast, imaging of long stabilization systems may be more challenging even with advanced sequences, particularly when transverse connections and vertebral or disc replacements are employed.[124,129] New carbon stabilization systems produce
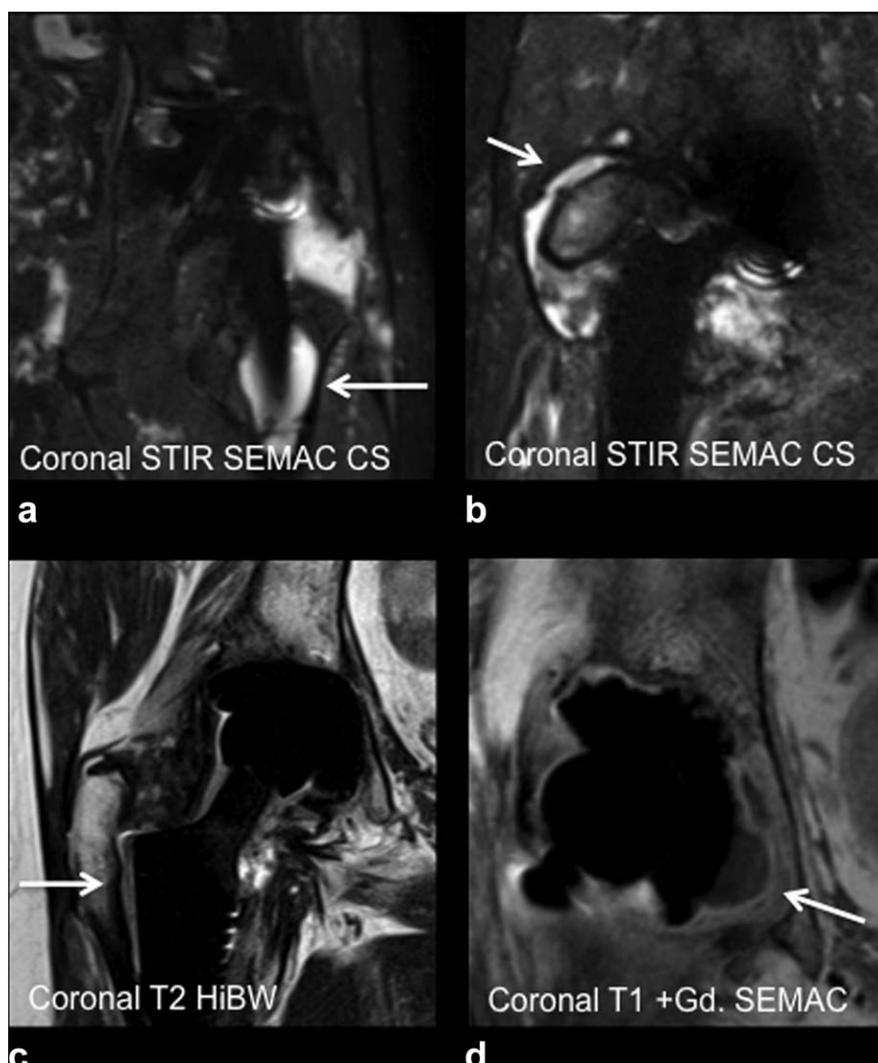
FIGURE 6: Important complications around metal implants. Arrows indicate respective pathologies. a: Periprosthetic osteolysis in a patient with a total hip arthroplasty. b: Pseudotumor formation (adverse local tissue reactions (ALTR)) around a metal-on-metal hip arthroplasty. c: Aseptic loosening of a total hip arthroplasty. d: Abscess formation adjacent to a proximal femur replacement. STIR, short tau inversion recovery; SEMAC, slice-encoding for metal artifact correction; CS, compressed sensing; HiBW, high bandwidth; Gd., Gadolinium.

fewer artifacts on CT and MRI. Besides the aforementioned complications, typical clinical queries are postoperative intradural or epidural hematoma, abscess or tumor, spondylodiscitis, neuroforaminal stenosis, disc protrusion, or myelopathy.[124,125]

Shoulder

MARS imaging can successfully be performed at the shoulder.[3,105,130–133] However, since the shoulder is not located in the isocenter of the main magnetic field but peripherally with a more inhomogeneous magnetic field, severe inhomogeneity artifacts are encountered.[132,134] Additionally, spherical components such as the humeral head replacement cause typical cloverleaf artifacts.[132,134] In cases with nonmetallic implants or suture anchors, standard sequences may be used successfully. If larger artifacts are encountered or specific

questions with respect to the metal implant are supposed to be answered, advanced MARS sequences are required.

Evaluation of the integrity of rotator cuff tendons and muscles is a frequent question after rotator cuff repair and after open reduction internal fixation (ORIF) of a proximal humerus fracture (Figs. (5 and 7)).[105,133] Function and integrity of the rotator cuff is essential after implantation of an anatomical shoulder prosthesis.[135] Subscapularis rupture and fatty infiltration as a common late cause of anterior instability following shoulder arthroplasty may be evaluated on MARS images.[105] Evaluation of the integrity, atrophy, and fatty infiltration of the delta muscle are important before and after reverse shoulder arthroplasty.[105] Attention needs to be paid to the acromion after reverse arthroplasty to exclude fractures or stress reactions that are common at these locations.[136] Bone marrow edema and loosening may specifically be observed at the inferior glenoid in case of
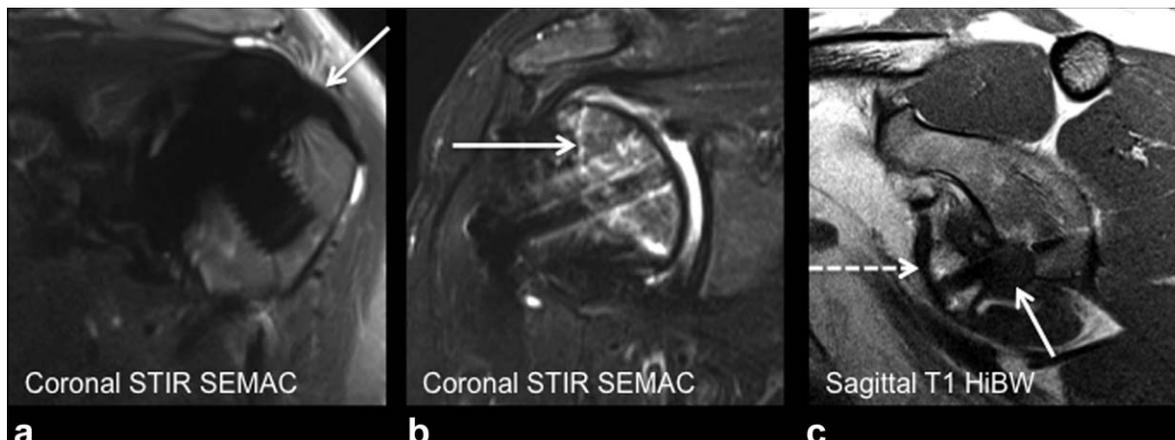
FIGURE 7: Examples of MARS sequences for shoulder MRI. a: Patient with a shoulder hemiarthroplasty. The supraspinatus tendon and its insertion can nicely be depicted (arrow). b: Patient with a Philos plate for a proximal humeral fracture. The demarcation line of a humeral head necrosis can be depicted without difficulty (arrow). c: Patient with a Latarjet procedure and a broken screw. The transferred coracoid process (dashed arrow) shows no osseous consolidation to the glenoid and a fluid formation in the osseous gap (arrow).

anatomical or reversed arthroplasties. In case of isolated replacement of the humeral head (shoulder hemiarthroplasty; anatomical glenoid remains), glenoid osteoarthritis may be observed during follow-up.[137] In patients with shoulder instability, bone consolidation between the glenoid and the transferred coracoid process may be evaluated after the Latarjet procedure (Fig. 7). More frequently than in other joints, synovitis and adhesive capsulitis (frozen shoulder) are observed postoperatively.

Elbow/Wrist/Hand

At the elbow and at the wrist, joint prostheses are rare (Fig. 8).[60] Screws for fracture fixation or ligament reattachment are found more commonly. While small scaphoid screws

may be imaged without major limitations, more complex hardware such as the frequent palmar ORIF for distal radius fractures causes more severe artifacts even when using advanced techniques. Concomitant injuries to cartilage, ligaments or triangular disc as well as carpal injuries or posttraumatic osteoarthritis may be depicted on MARS imaging.[138,139]

Hip

The hip joint represents the joint that is imaged most frequently with MARS sequences (Fig. 9).[115] MAVRIC has been shown to be more sensitive than standard TSE sequences for determining the volume of osteonecrosis of the femoral head in patients with instrumentations for femoral neck
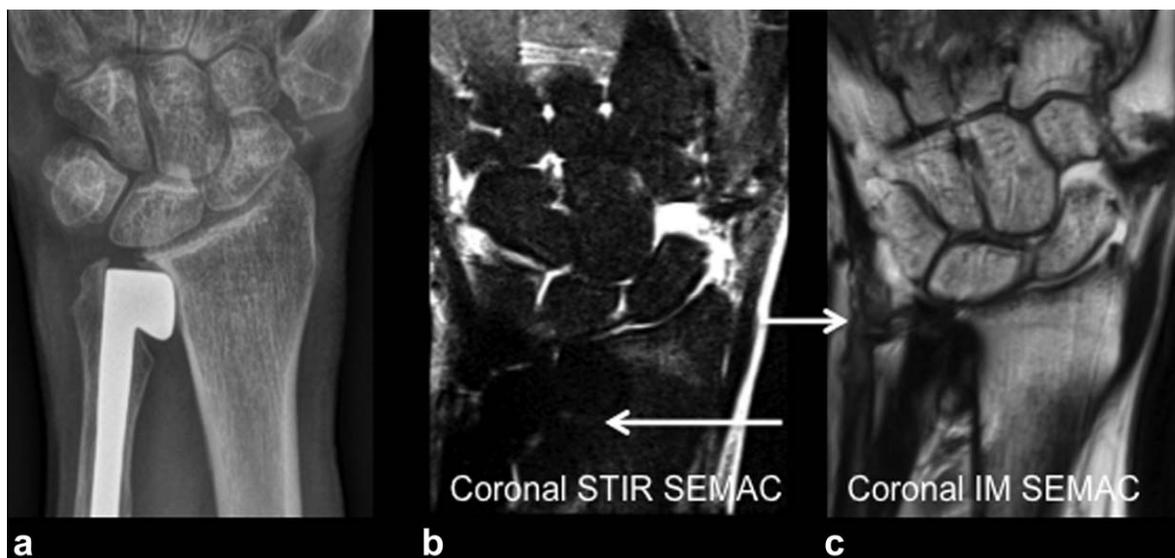

FIGURE 8: MARS sequences for MRI of the distal forearm. In a patient with an ulnar head prosthesis (a), STIR SEMAC images still demonstrate substantial artifacts around the prosthesis (b, arrow), whereas the rest of the image features a stable fat saturation. On intermediate weighted SEMAC sequences without fat saturation (c) the triangular fibrocartilage complex (TFCC; arrow) and the proximal carpal row are depicted nicely. STIR, short tau inversion recovery; SEMAC, slice-encoding for metal artifact correction; IM, intermediate weighted.
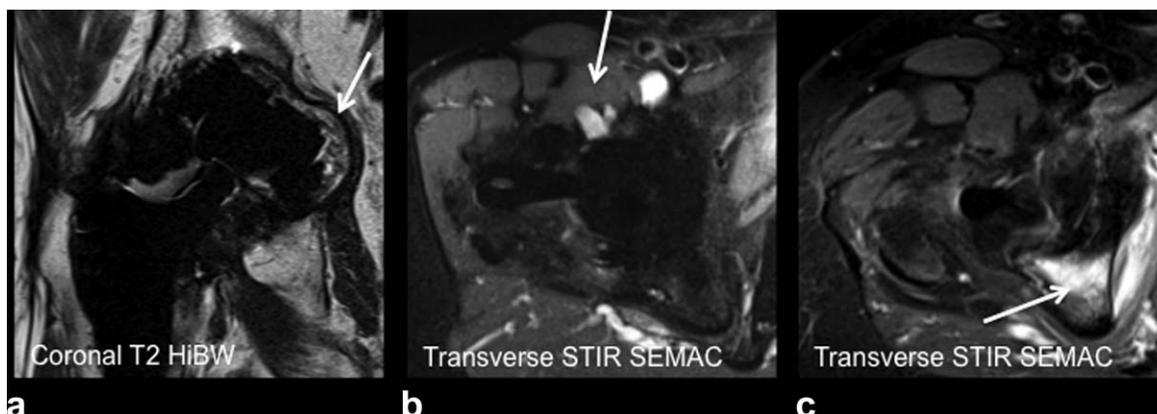
FIGURE 9: Examples of MARS sequences for hip MRI in patients with total hip arthroplasties. a: Extensive osteolysis of the acetabulum. b: Iliopsoas bursitis. c: Postoperative bone marrow edema posterior to the acetabular cup.

fractures.[140] But most reports on the utility of MARS imaging are on hip prostheses, since total hip arthroplasty (THA) is the most commonly performed prosthesis implantation.[10,49,117,118,141–143] MSI imaging has been shown to be clinically relevant for imaging of THA[1]: Almost half of the abnormal imaging findings were missed on STIR-high bandwidth sequences compared with STIR-SEMAC images, while T_1-high bandwidth imaging was similar to T_1-SEMAC imaging.[1] MARS imaging of THA became

particularly relevant due to severe complications after metal-on-metal hip prostheses. In the algorithmic approach to diagnosis and management of metal-on-metal arthroplasty published in 2012 by the hip society,[113] imaging should include ultrasound or metal artifact reduction sequence MRI in addition to plain radiography.[113,114,144,145] MARS sequences including VAT and SEMAC have been shown to be useful for detection, staging, and progression analyses of adverse local tissue reactions (ALTR) in the context of
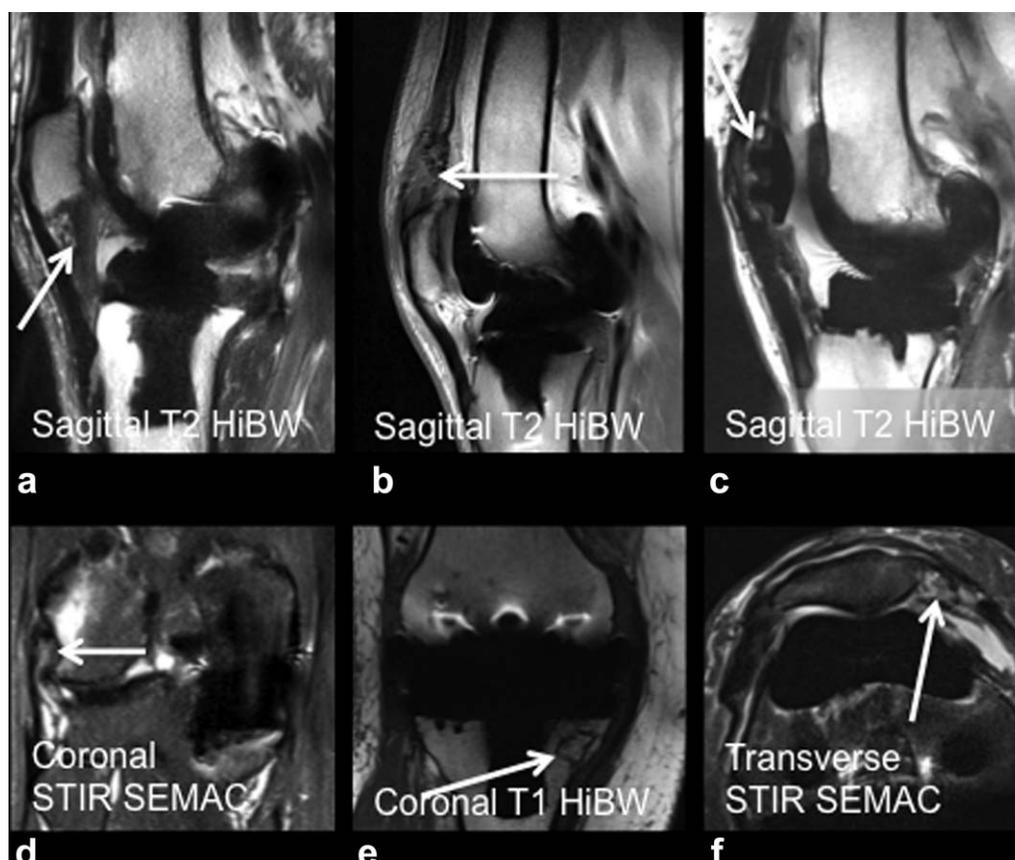

FIGURE 10: Examples of MARS sequences for knee MRI in patients with total (a–c, e–f) knee arthroplasty or unicompartimental (d) knee arthroplasty. a: Arthrofibrosis. b: Rupture of the quadriceps tendon. c: Loosening of the patella replacement. d: Proximal rupture of the lateral collateral ligament. e: Bone infarct. f: Rupture of the medial patellofemoral ligament. HiBW, high bandwidth; STIR, short tau inversion recovery; SEMAC, slice-encoding for metal artifact correction.

FIGURE 11: Examples of MARS sequences for foot and ankle MRI. While in patients with suture-button fixation of the syndesmosis standard MR protocols may be used and artifacts do not obscure the joint space (a) in patients with screw fixation of the medial malleolus fat saturation fails and severe artifacts occur on standard intermediate weighted sequences with spectral fat saturation (b), MARS sequences are helpful in this case, depicting a bone marrow edema of the talus (c, arrow). d,e: Patient with internal fixation of a calcaneus fracture. The fracture line is depicted on T_1-weighted sequences with high bandwidth (arrow; d) and the bone marrow edema is depicted on STIR SEMAC images (arrow; e). IM, intermediate weighted; FS, fat saturated; STIR, short tau inversion recovery; VAT, view angle tilting; HiBW, high bandwidth; SEMAC, slice-encoding for metal artifact correction. Cor., coronal; sag., sagittal.

metal-on-metal hip prostheses.[53,110–115,146–152] Several studies reported ALTR findings on MRI in up to a third of asymptomatic patients, and despite missing laboratory findings, there is no significant relation between MRI findings and pain or a priori risk factors, which underlines the importance of MRI.[53,151–153] Other findings after THA include periprosthetic bone marrow edema, periprosthetic fracture, synovitis, infection, hemarthrosis, capsular thickening or adhesions, component displacement, heterotopic ossification, iliopsoas impingement, and bursitis or iliopsoas tendon rupture. An internal impingement may cause edematous changes in the piriformis muscle. Symptoms may

further arise from abductor tendon pathology, trochanteric bursitis, gluteal muscle atrophy, or fatty infiltration.[154]

Knee
After the hip, the knee is the second most frequently replaced joint.[2,44,155,156] MARS techniques work successfully at the knee despite the minor surrounding soft tissue and the more complex metal anatomy (Fig. 10).[61] For unilateral knee replacements, a clinical relevance was shown for SEMAC STIR sequences.[103] SEMAC STIR sequences were useful in detecting bone marrow edema and influenced the orthopedic surgeons' decisions towards surgery, while IM-

w SEMAC showed no clinical benefit.[103] IM-w SEMAC was worse in detecting meniscal lesions than the corresponding high-bandwidth sequence, underlining the importance of using a combination of appropriate sequences.[103]

In the presence of a TKA pseudotumors, osteolysis, loosening, periprosthetic fracture, and infection are frequent queries.[157] Other possible complications after TKA are arthrofibrosis, collateral ligament rupture, quadriceps tendon rupture, retropatellar osteoarthritis, and patellar clunk syndrome. Malalignment of the prosthetic components may also be appropriately measured using MARS MRI.[44] When performing knee MRI in the presence of other metal implants, it needs to be estimated how much the region of interest will be obscured by artifacts when using standard sequences: For example, in patients with anterior cruciate ligament reconstruction, metal implants only show metal artifacts and insufficient fat saturation right next to the implants but the rest of the knee joint may be evaluated sufficiently.

Ankle/Foot

A variety of foot and ankle surgeries comprise metal hardware implantation, such as internal fixation for fractures, realignment surgeries (eg, hallux valgus), or arthrodeses.[5] Cartilage restorative procedures often require osteotomy of the medial malleolus with consecutive screw fixation.[5] After syndesmosis reconstruction with suture button or after screw removal, usually standard MR sequences may be used without diagnostic restrictions with respect to cartilage or ligament evaluation (Fig. 11). It was shown that 1.5T and 3T MRI can be used for evaluation of the articular surface of the ankle, if titanium screws are at least 3 mm distant.[158] MRI with Dixon sequences and spoiled gradient-echo (SPGR) sequences enabled significantly improved visualization of articular cartilage in patients with metal implants of the ankle, with reduced metal artifacts and a more uniform fat saturation compared to frequency selective fat suppression.[57] However, no significant improvement was found in the visibility of ligaments.[57] On ankle MARS MRI, detection of osteochondral lesions, syndesmosis ruptures, osteoarthritis, nonunion of fractures or arthrodesis, tendon injury, or avascular necrosis of the talus is possible (Fig. 11).[5] At the foot, stress reactions with bone marrow edema, fractures, infection, abscess, and osteomyelitis can be diagnosed or excluded on MARS MRI after reconstructive surgeries with metal implants such as for hallux valgus or neuropathic arthropathy (Fig. 11).[5]

Other Applications

Besides orthopedic implants, other applications of MARS sequences in the presence of metal implants include radiotherapy planning close to implants,[159] cerebral MRI in the presence of intracranial aneurysm clips,[54,160] cardiac imaging,[161,162] odontics,[163–165] and breast imaging.[59] However, these fields are not covered in this review.

SUMMARY

In conclusion, MRI around metal has improved significantly in recent years. Knowing the characteristics of both the implant and the area to be visualized on MRI may considerably improve the image quality, since a suitable MR protocol can be chosen and adapted. Depending on the material composition, the configuration, and size of the metal implant and the implant orientation, the size of the metal artifacts on MRI varies substantially. For all techniques, 1.5T instead of 3T MR scanners are preferable in the presence of metal, although adequate image quality may also be obtained at 3T. Appropriate pulse sequences include TSE sequences instead of gradient echo sequences and STIR sequences or Dixon sequences instead of standard spectral fat saturation.

Strategies for optimizing standard sequences include increasing the receiver bandwidth and reducing the slice thickness and pixel size. Dedicated advanced metal artifact-reducing techniques such as VAT, MAVRIC, and SEMAC are currently being developed further and promise a strong metal artifact reduction in clinically reasonable scanning times, especially together with postprocessing reconstruction algorithms such as compressed sensing (iterative reconstruction) combined with undersampling. Using these techniques, MRI becomes feasible for most orthopedic implants. Yet the scan protocol necessitates individual adjustments in many patients to achieve an optimal image quality. The MR examinations always need be evaluated in conjunction with plane radiography. Since plane radiography provides a cost-effective, easily acquired overview of implants and bone (which is only visible indirectly on MRI), it remains the basis for monitoring patients in a long-term follow-up.

References

1. Sutter R, Ulbrich EJ, Jellus V, Nittka M, Pfirrmann CW. Reduction of metal artifacts in patients with total hip arthroplasty with slice-encoding metal artifact correction and view-angle tilting MR imaging. Radiology 2012;265:204–214.

2. Sutter R, Hodek R, Fucentese SF, Nittka M, Pfirrmann CW. Total knee arthroplasty MRI featuring slice-encoding for metal artifact correction: reduction of artifacts for STIR and proton density-weighted sequences. AJR Am J Roentgenol 2013;201:1315–1324.

3. Beltran LS, Bencardino JT, Steinbach LS. Postoperative MRI of the shoulder. J Magn Reson Imaging 2014;40:1280–1297.

4. Hayter CL, Koff MF, Shah P, Koch KM, Miller TT, Potter HG. MRI after arthroplasty: comparison of MAVRIC and conventional fast spin-echo techniques. AJR Am J Roentgenol 2011;197:W405–411.

5. Sofka CM. Postoperative magnetic resonance imaging of the foot and ankle. J Magn Reson Imaging 2013;37:556–565.

6. Vande Berg B, Malghem J, Maldague B, Lecouvet F. Multi-detector CT imaging in the postoperative orthopedic patient with metal hardware. Eur J Radiol 2006;60:470–479.

7. Jungmann PM, Ganter C, Schaeffeler CJ, et al. View-angle tilting and slice-encoding metal artifact correction for artifact reduction in MRI: experimental sequence optimization for orthopaedic tumor endoprostheses and clinical application. PLoS One 2015;10:e0124922.

8. Runge VM. Current technological advances in magnetic resonance with critical impact for clinical diagnosis and therapy. Invest Radiol 2013;48:869–877.

9. Buckwalter KA, Lin C, Ford JM. Managing postoperative artifacts on computed tomography and magnetic resonance imaging. Semin Musculoskelet Radiol 2011;15:309–319.

10. Fritz J, Lurie B, Miller TT, Potter HG. MR imaging of hip arthroplasty implants. Radiographics 2014;34:E106–132.

11. Dillenseger JP, Moliere S, Choquet P, Goetz C, Ehlinger M, Bierry G. An illustrative review to understand and manage metal-induced artifacts in musculoskeletal MRI: a primer and updates. Skeletal Radiol 2016;45:677–688.

12. Koff MF, Shah P, Potter HG. Clinical implementation of MRI of joint arthroplasty. AJR Am J Roentgenol 2014;203:154–161.

13. Ariyanayagam T, Malcolm PN, Toms AP. Advances in metal artifact reduction techniques for periprosthetic soft tissue imaging. Semin Musculoskelet Radiol 2015;19:328–334.

14. Graf H, Steidle G, Martirosian P, Lauer UA, Schick F. Metal artifacts caused by gradient switching. Magn Reson Med 2005;54:231–234.

15. Graf H, Steidle G, Martirosian P, Lauer UA, Schick F. Effects on MRI due to altered rf polarization near conductive implants or instruments. Med Phys 2006;33:124–127.

16. Graf H, Lauer UA, Berger A, Schick F. RF artifacts caused by metallic implants or instruments which get more prominent at 3 T: an in vitro study. Magn Reson Imaging 2005;23:493–499.

17. Koch KM, King KF, Carl M, Hargreaves BA. Imaging near metal: The impact of extreme static local field gradients on frequency encoding processes. Magn Reson Med 2014;71:2024–2034.

18. Hargreaves BA, Worters PW, Pauly KB, Pauly JM, Koch KM, Gold GE. Metal-induced artifacts in MRI. AJR Am J Roentgenol 2011;197:547–555.

19. Vashaee S, Goora F, Britton MM, Newling B, Balcom BJ. Mapping B(1)-induced eddy current effects near metallic structures in MR images: a comparison of simulation and experiment. J Magn Reson 2015;250:17–24.

20. Shellock FG, Karacozoff AM. Detection of implants and other objects using a ferromagnetic detection system: implications for patient screening before MRI. AJR Am J Roentgenol 2013;201:720–725.

21. Shellock FG, Spinazzi A. MRI safety update 2008: part 2, screening patients for MRI. AJR Am J Roentgenol 2008;191:1140–1149.

22. Shellock FG, Crues JV. MR procedures: biologic effects, safety, and patient care. Radiology 2004;232:635–652.

23. Imai H, Tanaka Y, Nomura N, et al. Three-dimensional quantification of susceptibility artifacts from various metals in magnetic resonance images. Acta Biomater 2013;9:8433–8439.

24. Bakker CJ, Bhagwandien R, Moerland MA, Fuderer M. Susceptibility artifacts in 2DFT spin-echo and gradient-echo imaging: the cylinder model revisited. Magn Reson Imaging 1993;11:539–548.

25. Koch KM, Hargreaves BA, Pauly KB, Chen W, Gold GE, King KF. Magnetic resonance imaging near metal implants. J Magn Reson Imaging 2010;32:773–787.

26. David FH, Grierson J, Lamb CR. Reducing susceptibility artefacts in magnetic resonance images of the canine stifle following surgery for cranial cruciate ligament deficiency. Vet Comp Orthop Traumatol 2012;25:488–497.

27. Eustace S, Jara H, Goldberg R, et al. A comparison of conventional spin-echo and turbo spin-echo imaging of soft tissues adjacent to orthopedic hardware. AJR Am J Roentgenol 1998;170:455–458.

28. Farrelly C, Davarpanah A, Brennan SA, Sampson M, Eustace SJ. Imaging of soft tissues adjacent to orthopedic hardware: comparison of 3-T and 1.5-T MRI. AJR Am J Roentgenol 2010;194:W60–64.

29. Gupta A, Subhas N, Primak AN, Nittka M, Liu K. Metal artifact reduction: standard and advanced magnetic resonance and computed tomography techniques. Radiol Clin North Am 2015;53:531–547.

30. Koff MF, Shah P, Koch KM, Potter HG. Quantifying image distortion of orthopedic materials in magnetic resonance imaging. J Magn Reson Imaging 2013;38:610–618.

31. Zou YF, Chu B, Wang CB, Hu ZY. Evaluation of MR issues for the latest standard brands of orthopedic metal implants: plates and screws. Eur J Radiol 2015;84:450–457.

32. Mansson S, Muller GM, Wellman F, Nittka M, Lundin B. Phantom based qualitative and quantitative evaluation of artifacts in MR images of metallic hip prostheses. Phys Med 2015;31:173–178.

33. Ahmad FU, Sidani C, Fourzali R, Wang MY. Postoperative magnetic resonance imaging artifact with cobalt-chromium versus titanium spinal instrumentation: presented at the 2013 Joint Spine Section Meeting. Clinical article. J Neurosurg Spine 2013;19:629–636.

34. Heyse TJ, Chong le R, Davis J, Boettner F, Haas SB, Potter HG. MRI analysis of the component-bone interface after TKA. Knee 2012;19:290–294.

35. Kim SC, Lee HJ, Son SG, et al. Aluminum-free low-modulus Ti-C composites that exhibit reduced image artifacts during MRI. Acta Biomater 2015;12:322–331.

36. Jin Z, Guan Y, Yu G, Sun Y. Magnetic resonance imaging of postoperative fracture healing process without metal artifact: a preliminary report of a novel animal model. Biomed Res Int 2016;2016:1429892.

37. Zimel MN, Hwang S, Riedel ER, Healey JH. Carbon fiber intramedullary nails reduce artifact in postoperative advanced imaging. Skeletal Radiol 2015;44:1317–1325.

38. Ernstberger T, Buchhorn G, Heidrich G. Artifacts in spine magnetic resonance imaging due to different intervertebral test spacers: an in vitro evaluation of magnesium versus titanium and carbon-fiber-reinforced polymers as biomaterials. Neuroradiology 2009;51:525–529.

39. Filli L, Luechinger R, Frauenfelder T, et al. Metal-induced artifacts in computed tomography and magnetic resonance imaging: comparison of a biodegradable magnesium alloy versus titanium and stainless steel controls. Skeletal Radiol 2015;44:849–856.

40. Trammell TR, Flint K, Ramsey CJ. A comparison of MRI and CT imaging clarity of titanium alloy and titanium alloy with cobalt-chromium-alloy pedicle screw and rod implants in the lumbar spine. J Bone Joint Surg Am 2012;94:1479–1483.

41. Feng DX, McCauley JP, Morgan-Curtis FK, et al. Evaluation of 39 medical implants at 7.0 T. Br J Radiol 2015;88:20150633.

42. .Dula AN, Virostko J, Shellock FG. Assessment of MRI issues at 7 T for 28 implants and other objects. AJR Am J Roentgenol 2014;202:401–405.

43. Lee MJ, Kim S, Lee SA, et al. Overcoming artifacts from metallic orthopedic implants at high-field-strength MR imaging and multi-detector CT. Radiographics 2007;27:791–803.

44. Chang EY, Bae WC, Chung CB. Imaging the knee in the setting of metal hardware. Magn Reson Imaging Clin N Am 2014;22:765–786.

45. Takeuchi N, Mitsuyasu H, Nakanishi T, et al. The orientation of orthopaedic metallic devices relative to the frequency-encoding gradient affects susceptibility artifacts: an experiment using open MR imaging. Fukuoka Igaku Zasshi 2011;102:185–194.

46. Buckwalter KA. Optimizing imaging techniques in the postoperative patient. Semin Musculoskelet Radiol 2007;11:261–272.

47. Vandevenne JE, Vanhoenacker FM, Parizel PM, Butts Pauly K, Lang RK. Reduction of metal artefacts in musculoskeletal MR imaging. JBR-BTR 2007;90:345–349.

48. Gerigk L, Bostel T, Hegewald A, et al. Dynamic magnetic resonance imaging of the cervical spine with high-resolution 3-dimensional T2-imaging. Clin Neuroradiol 2012;22:93–99.

49. Talbot BS, Weinberg EP. MR imaging with metal-suppression sequences for evaluation of total joint arthroplasty. Radiographics 2016;36:209–225.

50. Bley TA, Wieben O, Francois CJ, Brittain JH, Reeder SB. Fat and water magnetic resonance imaging. J Magn Reson Imaging 2010;31:4–18.

51. Lee YH, Hahn S, Kim E, Suh JS. Fat-suppressed MR imaging of the spine for metal artifact reduction at 3T: comparison of STIR and slice-encoding for metal artifact correction fat-suppressed T2-weighted images. Magn Reson Med Sci 2016;15:371–378.

52. Ulbrich EJ, Sutter R, Aguiar RF, Nittka M, Pfirrmann CW. STIR sequence with increased receiver bandwidth of the inversion pulse for reduction of metallic artifacts. AJR Am J Roentgenol 2012;199:W735–742.

53. Muller GM, Mansson S, Muller MF, et al. MR imaging with metal artifact-reducing sequences and gadolinium contrast agent in a case-control study of periprosthetic abnormalities in patients with metal-on-metal hip prostheses. Skeletal Radiol 2014;43:1101–1112.

54. Kochan M, Daga P, Burgos N, et al. Simulated field maps for susceptibility artefact correction in interventional MRI. Int J Comput Assist Radiol Surg 2015;10:1405–1416.

55. Cha JG, Hong HS, Park JS, Paik SH, Lee HK. Practical application of iterative decomposition of water and fat with echo asymmetry and least-squares estimation (IDEAL) imaging in minimizing metallic artifacts. Korean J Radiol 2012;13:332–341.

56. Cha JG, Jin W, Lee MH, et al. Reducing metallic artifacts in postoperative spinal imaging: usefulness of IDEAL contrast-enhanced T1- and T2-weighted MR imaging—phantom and clinical studies. Radiology 2011;259:885–893.

57. Lee JB, Cha JG, Lee MH, Lee YK, Lee EH, Jeon CH. Usefulness of IDEAL T2-weighted FSE and SPGR imaging in reducing metallic artifacts in the postoperative ankles with metallic hardware. Skeletal Radiol 2013;42:239–247.

58. Murakami M, Mori H, Kunimatsu A, et al. Postsurgical spinal magnetic resonance imaging with iterative decomposition of water and fat with echo asymmetry and least-squares estimation. J Comput Assist Tomogr 2011;35:16–20.

59. Le Y, Kipfer HD, Majidi SS, Holz S, Lin C. Comparison of the artifacts caused by metallic implants in breast MRI using dual-echo dixon versus conventional fat-suppression techniques. AJR Am J Roentgenol 2014;203:W307–314.

60. Johnson D, Stevens KJ, Riley G, Shapiro L, Yoshioka H, Gold GE. Approach to MR imaging of the elbow and wrist: technical aspects and innovation. Magn Reson Imaging Clin N Am 2015;23:355–366.

61. Bachschmidt TJ, Sutter R, Jakob PM, Pfirrmann CW, Nittka M. Knee implant imaging at 3 Tesla using high-bandwidth radiofrequency pulses. J Magn Reson Imaging 2015;41:1570–1580.

62. Kumar NM, de Cesar Netto C, Schon LC, Fritz J. Metal artifact reduction magnetic resonance imaging around arthroplasty implants: the negative effect of long echo trains on the implant-related artifact. Invest Radiol 2017 [Epub ahead of print].

63. Allison J, Yanasak N. What MRI sequences produce the highest specific absorption rate (SAR), and is there something we should be doing to reduce the SAR during standard examinations? AJR Am J Roentgenol 2015;205:W140.

64. Toms AP, Smith-Bateman C, Malcolm PN, Cahir J, Graves M. Optimization of metal artefact reduction (MAR) sequences for MRI of total hip prostheses. Clin Radiol 2010;65:447–452.

65. Carmichael DW, Thomas DL, Ordidge RJ. Reducing ghosting due to k-space discontinuities in fast spin echo (FSE) imaging by a new combination of k-space ordering and parallel imaging. J Magn Reson 2009;200:119–125.

66. Suh JS, Jeong EK, Shin KH, et al. Minimizing artifacts caused by metallic implants at MR imaging: experimental and clinical studies. AJR Am J Roentgenol 1998;171:1207–1213.

67. Cho ZH, Kim DJ, Kim YK. Total inhomogeneity correction including chemical shifts and susceptibility by view angle tilting. Med Phys 1988;15:7–11.

68. Koch KM, Lorbiecki JE, Hinks RS, King KF. A multispectral three-dimensional acquisition technique for imaging near metal implants. Magn Reson Med 2009;61:381–390.

69. Choi SJ, Koch KM, Hargreaves BA, Stevens KJ, Gold GE. Metal artifact reduction with MAVRIC SL at 3-T MRI in patients with hip arthroplasty. AJR Am J Roentgenol 2015;204:140–147.

70. Koch KM, Brau AC, Chen W, et al. Imaging near metal with a MAVRIC-SEMAC hybrid. Magn Reson Med 2011;65:71–82.

71. Ai T, Padua A, Goerner F, et al. SEMAC-VAT and MSVAT-SPACE sequence strategies for metal artifact reduction in 1.5T magnetic resonance imaging. Invest Radiol 2012;47:267–276.

72. Lu W, Pauly KB, Gold GE, Pauly JM, Hargreaves BA. SEMAC: Slice-encoding for metal artifact correction in MRI. Magn Reson Med 2009;62:66–76.

73. Liebl H, Heilmeier U, Lee S, et al. In vitro assessment of knee MRI in the presence of metal implants comparing MAVRIC-SL and conventional fast spin echo sequences at 1.5 and 3 T field strength. J Magn Reson Imaging 2015;41:1291–1299.

74. Reichert M, Ai T, Morelli JN, Nittka M, Attenberger U, Runge VM. Metal artefact reduction in MRI at both 1.5 and 3.0 T using slice-encoding for metal artefact correction and view angle tilting. Br J Radiol 2015;88:20140601.

75. Nardo L, Han M, Kretzschmar M, et al. Metal artifact suppression at the hip: diagnostic performance at 3.0 T versus 1.5 Tesla. Skeletal Radiol 2015;44:1609–1616.

76. Lazik A, Landgraeber S, Schulte P, Kraff O, Lauenstein TC, Theysohn JM. Usefulness of metal artifact reduction with WARP technique at 1.5 and 3T MRI in imaging metal-on-metal hip resurfacings. Skeletal Radiol 2015;44:941–951.

77. Koch KM, Koff MF, Shah PH, Kanwischer A, Gui D, Potter HG. Flexible longitudinal magnetization contrast in spectrally overlapped 3D-MSI metal artifact reduction sequences: Technical considerations and clinical impact. Magn Reson Med 2015;74:1349–1355.

78. Chen CA, Chen W, Goodman SB, et al. New MR imaging methods for metallic implants in the knee: artifact correction and clinical impact. J Magn Reson Imaging 2011;33:1121–1127.

79. Kretzschmar M, Nardo L, Han MM, et al. Metal artefact suppression at 3T MRI: comparison of MAVRIC-SL with conventional fast spin echo sequences in patients with Hip joint arthroplasty. Eur Radiol 2015;25:2403–2411.

80. Butts K, Pauly JM, Gold GE. Reduction of blurring in view angle tilting MRI. Magn Reson Med 2005;53:418–424.

81. Lu W, Pauly KB, Gold GE, Pauly JM, Hargreaves BA. Slice-encoding for metal artifact correction with noise reduction. Magn Reson Med 2011;65:1352–1357.

82. Deligianni X, Bieri O, Elke R, Wischer T, Egelhof T. Optimization of scan time in MRI for total hip prostheses: SEMAC tailoring for prosthetic implants containing different types of metals. Rofo 2015;187:1116–1122.

83. den Harder JC, van Yperen GH, Blume UA, Bos C. Ripple artifact reduction using slice overlap in slice-encoding for metal artifact correction. Magn Reson Med 2015;73:318–324.

84. Lee YH, Lim D, Kim E, Kim S, Song HT, Suh JS. Usefulness of slice-encoding for metal artifact correction (SEMAC) for reducing metallic artifacts in 3-T MRI. Magn Reson Imaging 2013;31:703–706.

85. Hargreaves BA, Chen W, Lu W, et al. Accelerated slice-encoding for metal artifact correction. J Magn Reson Imaging 2010;31:987–996.

86. Gold GE, Thedens DR, Pauly JM, et al. MR imaging of articular cartilage of the knee: new methods using ultrashort TEs. AJR Am J Roentgenol 1998;170:1223–1226.

87. Carl M, Koch K, Du J. MR imaging near metal with undersampled 3D radial UTE-MAVRIC sequences. Magn Reson Med 2013;69:27–36.

88. den Harder JC, van Yperen GH, Blume UA, Bos C. Off-resonance suppression for multispectral MR imaging near metallic implants. Magn Reson Med 2015;73:233–243.

89. Venook RD, Matter NI, Ramachandran M, et al. Prepolarized magnetic resonance imaging around metal orthopedic implants. Magn Reson Med 2006;56:177–186.

90. Ramos-Cabrer P, van Duynhoven JP, Van der Toorn A, Nicolay K. MRI of hip prostheses using single-point methods: in vitro studies towards the artifact-free imaging of individuals with metal implants. Magn Reson Imaging 2004;22:1097–1103.

91. Idiyatullin D, Corum C, Park JY, Garwood M. Fast and quiet MRI using a swept radiofrequency. J Magn Reson 2006;181:342–349.

92. Hoff MN, Xiang QS. An algebraic solution for banding artifact removal in bSSFP imaging. In: Proc 19th Annual Meeting ISMRM, Montreal; 2011. p 2416.

93. Hoff MN, Xiang QS. An XS-guided solution for bSSFP banding artifact correction with reduced scan time. In: Proc 20th Annual Meeting ISMRM, Melbourne; 2012. p 2416.

94. Xiang QS, Hoff MN. Simple cross-solution for banding artifact removal in bSSFP Imaging. In: Proc 18th Annual Meeting ISMRM, Stockholm; 2010. p 74.

95. Hoff MN, Green JD, Xiang QS. Imaging near metals with phase cycled SSFP. In: Proc 18th Annual Meeting ISMRM, Stockholm; 2010. p 3081.

96. Hoff MN, Xiang QS. Eliminating metal artifact distortion using 3D-PLACE. In: Proc 17th Annual Meeting ISMRM, Honolulu; 2009. p 570.

97. Skare S, Andersson JL. Correction of MR image distortions induced by metallic objects using a 3D cubic B-spline basis set: application to stereotactic surgical planning. Magn Reson Med 2005;54:169–181.

98. Worters PW, Sung K, Stevens KJ, Koch KM, Hargreaves BA. Compressed-sensing multispectral imaging of the postoperative spine. J Magn Reson Imaging 2013;37:243–248.

99. Fritz J, Fritz B, Thawait GK, et al. Advanced metal artifact reduction MRI of metal-on-metal hip resurfacing arthroplasty implants: compressed sensing acceleration enables the time-neutral use of SEMAC. Skeletal Radiol 2016;45:1345–1356.

100. Lustig M, Donoho D, Pauly JM. Sparse MRI: The application of compressed sensing for rapid MR imaging. Magn Reson Med 2007;58:1182–1195.

101. Fritz J, Ahlawat S, Demehri S, et al. Compressed sensing SEMAC: 8-fold accelerated high resolution metal artifact reduction MRI of cobalt-chromium knee arthroplasty implants. Invest Radiol 2016;51:666–676.

102. Otazo R, Nittka M, Bruno M, et al. Sparse-SEMAC: rapid and improved SEMAC metal implant imaging using SPARSE-SENSE acceleration. Magn Reson Med 2016 [Epub ahead of print].

103. Agten CA, Del Grande F, Fucentese SF, Blatter S, Pfirrmann CW, Sutter R. Unicompartmental knee arthroplasty MRI: impact of slice-encoding for metal artefact correction MRI on image quality, findings and therapy decision. Eur Radiol 2015;25:2184–2193.

104. Gutierrez LB, Do BH, Gold GE, et al. MR imaging near metallic implants using MAVRIC SL: initial clinical experience at 3T. Acad Radiol 2015;22:370–379.

105. Nwawka OK, Konin GP, Sneag DB, Gulotta LV, Potter HG. Magnetic resonance imaging of shoulder arthroplasty: review article. HSS J 2014;10:213–224.

106. Vessely MB, Frick MA, Oakes D, Wenger DE, Berry DJ. Magnetic resonance imaging with metal suppression for evaluation of periprosthetic osteolysis after total knee arthroplasty. J Arthroplasty 2006;21:826–831.

107. Waldstein W, Schmidt-Braekling T, Boettner F. MRI does not detect acetabular osteolysis around metal-on-metal Birmingham THA. Arch Orthop Trauma Surg 2014;134:1009–1015.

108. Robinson E, Henckel J, Sabah S, Satchithananda K, Skinner J, Hart A. Cross-sectional imaging of metal-on-metal hip arthroplasties. Can we substitute MARS MRI with CT? Acta Orthop 2014;85:577–584.

109. Walde TA, Weiland DE, Leung SB, et al. Comparison of CT, MRI, and radiographs in assessing pelvic osteolysis: a cadaveric study. Clin Orthop Relat Res 2005:138–144.

110. Madanat R, Hussey DK, Donahue GS, et al. Early lessons from a worldwide, multicenter, followup study of the recalled articular surface replacement hip system. Clin Orthop Relat Res 2016;474:166–174.

111. Lindgren K, Anderson MB, Peters CL, Pelt CE, Gililland JM. The prevalence of positive findings on metal artifact reduction sequence magnetic resonance imaging in metal-on-metal total hip arthroplasty. J Arthroplasty 2016;31:1519–1523.

112. Walsh CP, Hubbard JC, Nessler JP, Markel DC. MRI findings associated with recalled modular femoral neck rejuvenate and ABG implants. J Arthroplasty 2015;30:2021–2026.

113. Lombardi AV Jr, Barrack RL, Berend KR, et al. The Hip Society: algorithmic approach to diagnosis and management of metal-on-metal arthroplasty. J Bone Joint Surg Br 2012;94(11 Suppl A):14–18.

114. Kwon YM. Cross-sectional imaging in evaluation of soft tissue reactions secondary to metal debris. J Arthroplasty 2014;29:653–656.

115. Maloney E, Ha AS, Miller TT. Imaging of adverse reactions to metal debris. Semin Musculoskelet Radiol 2015;19:21–30.

116. Bisseling P, de Wit BW, Hol AM, van Gorp MJ, van Kampen A, van Susante JL. Similar incidence of periprosthetic fluid collections after ceramic-on-polyethylene total hip arthroplasties and metal-on-metal resurfacing arthroplasties: results of a screening metal artefact reduction sequence-MRI study. Bone Joint J 2015;97-B:1175–1182.

117. Hayter CL, Koff MF, Potter HG. Magnetic resonance imaging of the postoperative hip. J Magn Reson Imaging 2012;35:1013–1025.

118. Pilania K, Jankharia B. Magnetic resonance imaging features of complications following hip replacement: A pictorial review. Indian J Radiol Imaging 2016;26:271–278.

119. Susa M, Oguro S, Kikuta K, et al. Novel MR imaging method—MAVRIC—for metal artifact suppression after joint replacement in musculoskeletal tumor patients. BMC Musculoskelet Disord 2015;16:377.

120. Friedman T, Chen T, Chang A. MRI diagnosis of recurrent pigmented villonodular synovitis following total joint arthroplasty. HSS J 2013;9:100–105.

121. McLellan AM, Daniel S, Corcuera-Solano I, Joshi V, Tanenbaum LN. Optimized imaging of the postoperative spine. Neuroimaging Clin N Am 2014;24:349–364.

122. Han SB, Yoon YC, Kwon JW. Comparison study between conventional sequence and slice-encoding metal artifact correction (SEMAC) in the diagnosis of postoperative complications in patients receiving lumbar inter-body fusion and pedicle screw fixation surgery. PLoS One 2016;11:e0163745.

123. Stradiotti P, Curti A, Castellazzi G, Zerbi A. Metal-related artifacts in instrumented spine. Techniques for reducing artifacts in CT and MRI: state of the art. Eur Spine J 2009;18(Suppl 1):102–108.

124. Rutherford EE, Tarplett LJ, Davies EM, Harley JM, King LJ. Lumbar spine fusion and stabilization: hardware, techniques, and imaging appearances. Radiographics 2007;27:1737–1749.

125. Qi S, Wu ZG, Mu YF, et al. SEMAC-VAT MR imaging unravels peri-instrumentation lesions in patients with attendant symptoms after spinal surgery. Medicine (Baltimore) 2016;95:e3184.

126. Kaushik SS, Karr R, Runquist M, et al. Quantifying metal-induced susceptibility artifacts of the instrumented spine at 1.5T using fast-spin echo and 3D-multispectral MRI. J Magn Reson Imaging 2016;45:51–58.

127. Fuchs M, Putzier M, Pumberger M, Hermann KG, Diekhoff T. Acute vertebral fracture after spinal fusion: a case report illustrating the added value of single-source dual-energy computed tomography to magnetic resonance imaging in a patient with spinal instrumentation. Skeletal Radiol 2016;45:1303–1306.

128. Lee YH, Lim D, Kim E, Kim S, Song HT, Suh JS. Feasibility of fat-saturated T2-weighted magnetic resonance imaging with slice-

encoding for metal artifact correction (SEMAC) at 3T. Magn Reson Imaging 2014;32:1001–1005.

129. Elliott CA, Fox R, Ashforth R, Gourishankar S, Nataraj A. Magnetic resonance imaging artifact following anterior cervical discectomy and fusion with a trabecular metal cage. J Neurosurg Spine 2016;24: 496–501.

130. Pierce JL, Nacey NC, Jones S, et al. Postoperative shoulder imaging: rotator cuff, labrum, and biceps tendon. Radiographics 2016;36: 1648–1671.

131. Thakkar RS, Thakkar SC, Srikumaran U, McFarland EG, Fayad LM. Complications of rotator cuff surgery-the role of post-operative imaging in patient care. Br J Radiol 2014;87:20130630.

132. La Rocca Vieira R, Rybak LD, Recht M. Technical update on magnetic resonance imaging of the shoulder. Magn Reson Imaging Clin N Am 2012;20:149–161, ix.

133. Sperling JW, Potter HG, Craig EV, Flatow E, Warren RF. Magnetic resonance imaging of painful shoulder arthroplasty. J Shoulder Elbow Surg 2002;11:315–321.

134. Naraghi AM, White LM. Magnetic resonance imaging of joint replacements. Semin Musculoskelet Radiol 2006;10:98–106.

135. Mansat P, Bonnevialle N. Treatment of fracture sequelae of the proximal humerus: anatomical vs reverse shoulder prosthesis. Int Orthop 2015;39:349–354.

136. Farshad M, Gerber C. Reverse total shoulder arthroplasty-from the most to the least common complication. Int Orthop 2010;34:1075–1082.

137. Herschel R, Wieser K, Morrey ME, Ramos CH, Gerber C, Meyer DC. Risk factors for glenoid erosion in patients with shoulder hemiarthroplasty: an analysis of 118 cases. J Shoulder Elbow Surg 2016 [Epub ahead of print].

138. Klempka A, Wagner M, Fodor S, Prommersberger KJ, Uder M, Schmitt R. Injuries of the scapholunate and lunotriquetral ligaments as well as the TFCC in intra-articular distal radius fractures. Prevalence assessed with MDCT arthrography. Eur Radiol 2016;26:722–732.

139. Giwa L, Spacey K, Packer G. Management of a complex, multioperated intra-articular distal radius fracture. J Wrist Surg 2015;4:179–182.

140. Farshad-Amacker NA, Koff MF, Dyke JP, et al. Assessment of osteonecrosis in the presence of instrumentation for femoral neck fracture using contrast-enhanced MAVRIC sequence. HSS J 2016;12:51–58.

141. Fritz J, Lurie B, Miller TT. Imaging of hip arthroplasty. Semin Musculoskelet Radiol 2013;17:316–327.

142. Bolognesi MP, Ledford CK. Metal-on-metal total hip arthroplasty: patient evaluation and treatment. J Am Acad Orthop Surg 2015;23: 724–731.

143. Ries MD, Link TM. Monitoring and risk of progression of osteolysis after total hip arthroplasty. Instr Course Lect 2013;62:207–214.

144. Campe CB, Palmer WE. MR imaging of metal-on-metal hip prostheses. Magn Reson Imaging Clin N Am 2013;21:155–168.

145. Ebreo D, Bell PJ, Arshad H, Donell ST, Toms A, Nolan JF. Serial magnetic resonance imaging of metal-on-metal total hip replacements. Follow-up of a cohort of 28 mm Ultima TPS THRs. Bone Joint J 2013;95-B:1035–1039.

146. Briant-Evans TW, Lyle N, Barbur S, et al. A longitudinal study of MARS MRI scanning of soft-tissue lesions around metal-on-metal total hip arthroplasties and disease progression. Bone Joint J 2015; 97-B:1328–1337.

147. Kwon YM, Liow MH, Dimitriou D, Tsai TY, Freiberg AA, Rubash HE. What is the natural history of "asymptomatic" pseudotumours in metal-on-metal hip arthroplasty? Minimum 4-year metal artifact reduction sequence magnetic resonance imaging longitudinal study. J Arthroplasty 2016;31(9 Suppl):121–126.

148. Kwon YM, Dimitriou D, Liow MH, Tsai TY, Li G. Is ultrasound as useful as metal artifact reduction sequence magnetic resonance imaging in longitudinal surveillance of metal-on-metal hip arthroplasty patients? J Arthroplasty 2016;31:1821–1827.

149. Koziara CR, Lombardo DJ, Petersen-Fitts GR, Jildeh TR, Morawa L. Effects of cobalt and chromium levels following modular hip stem total hip arthroplasty. Orthopedics 2016;39:288–292.

150. Goldstein JM, Fehring TK, Fehring KA. Cystic adverse local tissue reactions in asymptomatic modular metal-on-metal total hips may decrease over time. J Arthroplasty 2016;31:1589–1594.

151. Macnair RD, Wynn-Jones H, Wimhurst JA, Toms A, Cahir J. Metal ion levels not sufficient as a screening measure for adverse reactions in metal-on-metal hip arthroplasties. J Arthroplasty 2013;28:78–83.

152. Hart AJ, Satchithananda K, Liddle AD, et al. Pseudotumors in association with well-functioning metal-on-metal hip prostheses: a case-control study using three-dimensional computed tomography and magnetic resonance imaging. J Bone Joint Surg Am 2012;94:317–325.

153. Fehring TK, Odum S, Sproul R, Weathersbee J. High frequency of adverse local tissue reactions in asymptomatic patients with metal-on-metal THA. Clin Orthop Relat Res 2014;472:517–522.

154. Agten CA, Sutter R, Dora C, Pfirrmann CW. MR imaging of soft tissue alterations after total hip arthroplasty: comparison of classic surgical approaches. Eur Radiol 2016 [Epub ahead of print].

155. Sneag DB, Bogner EA, Potter HG. Magnetic resonance imaging evaluation of the painful total knee arthroplasty. Semin Musculoskelet Radiol 2015;19:40–48.

156. Fritz J, Lurie B, Potter HG. MR imaging of knee arthroplasty implants. Radiographics 2015;35:1483–1501.

157. Plodkowski AJ, Hayter CL, Miller TT, Nguyen JT, Potter HG. Lamellated hyperintense synovitis: potential MR imaging sign of an infected knee arthroplasty. Radiology 2013;266:256–260.

158. Radzi S, Cowin G, Robinson M, et al. Metal artifacts from titanium and steel screws in CT, 1.5T and 3T MR images of the tibial Pilon: a quantitative assessment in 3D. Quant Imaging Med Surg 2014;4: 163–172.

159. Schmidt MA, Panek R, Colgan R, et al. Slice-encoding for metal artefact correction in magnetic resonance imaging examinations for radiotherapy planning. Radiother Oncol 2016;120:356–362.

160. Friedrich B, Wostrack M, Ringel F, et al. Novel metal artifact reduction techniques with use of slice-encoding metal artifact correction and view-angle tilting MR imaging for improved visualization of brain tissue near intracranial aneurysm clips. Clin Neuroradiol 2016;26:31–37.

161. Olivieri LJ, Cross RR, O'Brien KE, Ratnayaka K, Hansen MS. Optimized protocols for cardiac magnetic resonance imaging in patients with thoracic metallic implants. Pediatr Radiol 2015;45:1455–1464.

162. Saeedi M, Thomas A, Shellock FG. Evaluation of MRI issues at 3-Tesla for a transcatheter aortic valve replacement (TAVR) bioprosthesis. Magn Reson Imaging 2015;33:497–501.

163. Beau A, Bossard D, Gebeile-Chauty S. Magnetic resonance imaging artefacts and fixed orthodontic attachments. Eur J Orthod 2015;37: 105–110.

164. Cortes AR, Abdala-Junior R, Weber M, Arita ES, Ackerman JL. Influence of pulse sequence parameters at 1.5 T and 3.0 T on MRI artefacts produced by metal-ceramic restorations. Dentomaxillofac Radiol 2015;44:20150136.

165. Zho SY, Kim MO, Lee KW, Kim DH. Artifact reduction from metallic dental materials in T1-weighted spin-echo imaging at 3.0 Tesla. J Magn Reson Imaging 2013;37:471–478.